Title

Reconstitution of kinetochore motility and microtubule dynamics reveals an interdependence of a microtubule polymerase and a motor protein in establishment of kinetochore end-on attachments

Author

Torvi, Julia

Publication Date

2023

Peer reviewed|Thesis/dissertation

Reconstitution of kinetochore motility and microtubule dynamics reveals an interdependence of a microtubule polymerase and a motor protein in establishment of kinetochore end-on attachments

By

Julia Torvi

A dissertation submitted in partial satisfaction of the

requirements for the degree of

Doctor of Philosophy

in

Biophysics

in the

Graduate Division

of the

University of California, Berkeley

Committee in charge:

Professor Georjana Barnes, Co-Chair
Professor David Drubin, Co-Chair
Professor Ahmet Yildiz
Professor Eva Nogales
Professor Rebecca Heald

Summer 2023

Reconstitution of kinetochore motility and microtubule dynamics reveals an interdependence of a microtubule polymerase and a motor protein in establishment of kinetochore end-on attachments

By
Julia Torvi

Abstract

Reconstitution of kinetochore motility and microtubule dynamics reveals an interdependence of a microtubule polymerase and a motor protein in establishment of kinetochore end-on attachments

By

Julia Torvi

Doctor of Philosophy in Biophysics

University of California, Berkeley

Professor Georjana Barnes, Co-Chair
Professor David Drubin, Co-Chair

During mitosis, individual microtubules make attachments to chromosomes via a specialized protein complex called the kinetochore to faithfully segregate the chromosomes to daughter cells. Translocation of kinetochores on the lateral surface of the microtubule has been proposed to contribute to high fidelity chromosome capture and alignment at the mitotic midzone, but has been difficult to observe in vivo because of spatial and temporal constraints. To overcome these barriers, we used total internal reflection fluorescence (TIRF) microscopy to track the interactions between microtubules, kinetochore proteins, and other microtubule-associated proteins in lysates from metaphase-arrested *Saccharomyces cerevisiae*. TIRF microscopy and cryo-correlative light microscopy and electron tomography indicated that we successfully reconstituted interactions between intact kinetochores and microtubules. These kinetochores translocate on the lateral microtubule surface toward the microtubule plus end and transition to end-on attachment, whereupon microtubule depolymerization commences.

These kinetochore dynamics we were able to reconstitute *in vitro* resembled the process of chromosome congression seen in cells. Chromosome alignment on the mitotic spindle, also referred to as congression, is facilitated by translocation of side-bound chromosomes along the microtubule surface, which allows the establishment of end-on attachment of kinetochores to microtubule plus ends. This is exactly what we observed in our reconstitution assay. We observed kinetochore translocation on the lateral microtubule surface toward the microtubule plus end, which we found that the directional kinetochore movement is dependent on the highly processive kinesin-8, Kip3. We propose that Kip3 facilitates stable kinetochore attachment to microtubule plus ends through its abilities to move the kinetochore laterally on the surface of the microtubule and to regulate microtubule plus end dynamics. Additionally, we also observed kinetochore motility was dependent on Stu2. However, we showed that these proteins display distinct dynamics on the microtubule. Kip3 is highly processive and moves faster

than the kinetochore. Stu2 tracks both growing and shrinking microtubule ends but also colocalizes with moving lattice-bound kinetochores. In cells, we observed that both Kip3 and Stu2 are important for establishing chromosome biorientation, Moreover, when both proteins are absent, biorientation is completely defective. All cells lacking both Kip3 and Stu2 had declustered kinetochores and about half also had at least one unattached kinetochore. Our evidence argues that despite differences in their dynamics, Kip3 and Stu2 share roles in chromosome congression to facilitate proper kinetochore-microtubule attachment.

Table of Contents

List of Figures

Acknowledgements

I keep trying to write an insightful and heartfelt history of my journey with mitosis, but nothing can even come close to summarizing the immense gratitude and appreciation for all the friends I've made along the way. So, I'll keep it short and sweet. To Jason and Haein for supporting me as a human and as a scientist. You gave me the support and training that set this whole thing in motion. To Matt for dealing with me as a bay-mate and friend for almost seven years now. You've always pushed me to be the best scientist I could be and without that I certainly wouldn't have come this far. Also thank you to McKenna because even though she probably doesn't know it, she was also part of our friendship. Thank you to Rena for joining our bay with such an unapologetic and strong sense of self. Our friendship has given me so much confidence in myself, to really open up and become *JULIA*. And to Jake, the friend who I've known for over six years now, but yet I still barely know anything about the SAC. Sometimes friendship is just love and support, not sharing the nitty gritty science details with. With that I also have to add my other SAC Gemini, Kostas. You've given me so much confidence, love, and support to just be *me*.

To the Drubin & Barnes lab, past and present, you made this whole PhD experience so wonderful and positive. I sincerely looked forward to coming into the lab every day, and that's because of you all. Ross and Michelle, while we only shared a small part of my time here in the lab together, we've shared so much outside of the lab, outdoors adventures, ski trips, etc. that I know we will continue into the future. To all my fellow grad students with me on this journey, Bob, Sam, Paul, Cyna, Jennifer, Max and Yui, we've got this!! You've got this!!! I know going through this all together means we will be friends for life. I love you all. Zane, I don't think you know how much our time as bay-mates has impacted me. I am weird, loud, and kind of a lot, and you're the first person who I feel like saw that and not only accepted it but also embraced it? Also, did you know Fiji is just imageJ? Jonathan, I can never figure out how to thank you appropriately. I think you know how thankful, appreciative, grateful, and happy I am to have shared my PhD with you, so let's just go with that. You're the dream science partner, so thank you. Lastly, thank you to David and Georjana for making this all possible, supporting me on this journey, and bringing in so many amazing people to work with in the lab. I am so proud of this thesis and I cannot thank you all enough for being there and supporting me on this journey. THE TRUTH IS OUT THERE!

Chapter One

Reconstitution of kinetochore motility and microtubule dynamics reveals a role for a kinesin-8 in establishing end-on attachments

1.1 Introduction

1.1.1 Mitosis and chromosome congression

During mitosis, a cell's replicated chromosomes are equally segregated to two daughter cells. In order for this process to happen accurately and efficiently, the microtubule cytoskeleton must completely remodel to form a bipolar spindle. Replicated chromosomes then attach to microtubules, emanating from opposite spindle poles, through a large dynamic chromosome-associated protein complex called the kinetochore. Proper kinetochore-microtubule attachment is vital for preservation of genomic integrity and prevention of cancer and birth defects (Weaver and Cleveland, 2005). Therefore, kinetochore attachment is highly regulated and tightly controlled (Tanaka, 2013).

During establishment of biorientation, kinetochores have been observed to first attach to the lateral surface of a microtubule (Tanaka, 2012). Such kinetochores then must be transported along the microtubule lattice, where they transition to an appropriate, and stable, end-on attachment (Rieder and Alexander, 1990; Tanaka *et al.*, 2005; Kapoor *et al.*, 2006). It is only after each sister kinetochore makes a proper end-on attachment with microtubules from opposite spindle poles that the cell will progress into anaphase and complete mitosis. This lateral to end-on attachment conversion has been observed in several eukaryotic species (Magidson *et al.*, 2015; Maiato *et al.*, 2017), but the underlying mechanisms have been elusive due both to the difficulty of observing this event *in vivo* and to biochemical hurdles *in vitro*.

Establishment of end-on kinetochore attachments to microtubules, for chromosomes that are initially attached to spindle microtubules laterally, can be divided into two processes: (1) chromosome lateral movement along the microtubule surface, and (2) conversion from lateral to end-on attachment. With regard to the kinetochore reaching the microtubule tip, CENP-E and chromokinesins are particularly important for chromosome movement to the spindle midzone in metazoans (Lemura and Tanaka, 2015; Craske and Welburn, 2020). However, fungi do not appear to have kinesin-7 or chromokinesin orthologs. Lateral to end-on conversion has been observed in fungi, but these events required that a depolymerizing microtubule tip meet the laterally bound kinetochore (Kalantzaki *et al.*, 2015). Other studies in fungi have also implicated minus-end directed motor-based transport of unattached kinetochores (Tanaka *et al.*, 2005), similar to a proposed metazoan mechanism involving the motor protein dynein and the mitotic spindle protein NuMA (Kapoor *et al.*, 2006; Li *et al.*, 2007) (Figure 1.1).

One class of proteins that might be involved in lateral kinetochore movements is the kinesin-8 motor proteins. This family of proteins includes key regulators of

kinetochore-microtubule dynamics. Through a dual-mode mechanism of destabilizing growing microtubules and stabilizing depolymerizing microtubules, kinesin-8 proteins have been proposed to tune microtubule dynamics for proper chromosome segregation (Risteski *et al.*, 2021). In budding yeast, Kip3, a highly processive kinesin-8, is required for kinetochore clustering into two discrete foci at metaphase, but how this activity relates to establishment of end-on attachments is not clear (Wargacki *et al.*, 2010; Su *et al.*, 2011). Declustered kinetochores may represent misaligned or defectively attached chromosomes (Shimogawa *et al.*, 2010; Wargacki *et al.*, 2010; Edzuka and Goshima, 2019). Additionally, in yeast that lack Kip3, chromosomes lag behind the main chromosome mass during anaphase (Tytell and Sorger, 2006, p. 200). The metazoan kinesin-8, Kif18a, is responsible for tuning kinetochore-microtubule dynamics, which ultimately affects chromosome alignment and equal segregation into the daughter cells (Stumpff *et al.*, 2008, 2012). Lagging chromosomes are common in cells lacking Kif18a and result in micronuclei formation (Fonseca *et al.*, 2019). Additionally, the Drosophila kinesin-8, Klp67A, shares many of the roles of other kinesin-8 proteins including stabilizing and destabilizing microtubules, but this kinesin also stabilizes kinetochore-microtubule attachments (Edzuka and Goshima, 2019). Taken together, these observations indicate that kinesin-8 motor proteins have roles both in regulating microtubule dynamics and in establishing kinetochore-microtubule attachments, while potentially playing a role in the formation of proper end-on attachments.

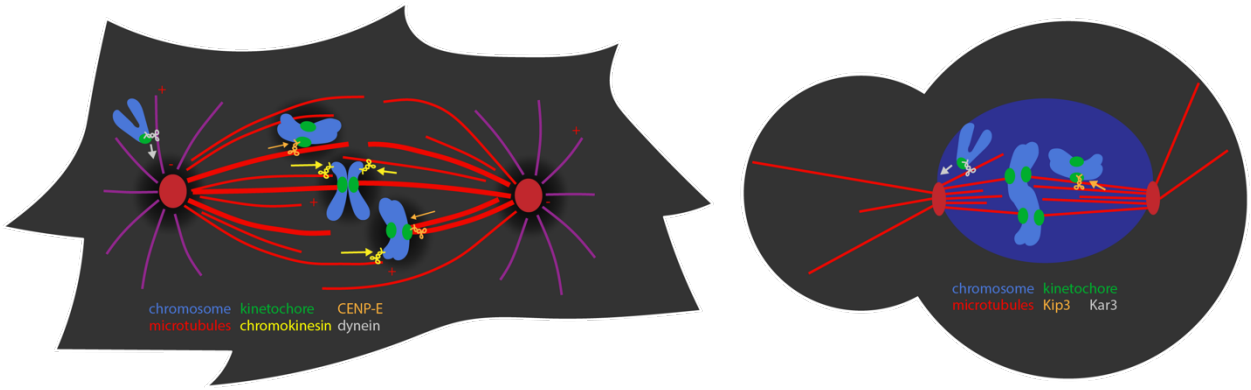

Figure 1.1 Mitosis in mammals vs. yeast. Two cells undergo chromosome congression during mitosis. On the left, a mammalian cell, which has an open mitosis attaches microtubules, in red, to the kinetochore, in green. These kinetochore microtubules, or k-fibers, are differently post-translationally modified for motor track specification. Dynein, in gray, walks on astral microtubules, moving kinetochores back to the centromeres. On k-fibers, chromokinesins push on chromosome arms and CENP-E bind the kinetochore, both pushing chromosomes towards the plus end of the microtubule and the metaphase plate. On the right, in budding yeast, there is a closed mitosis and microtubules are not differentially post-translationally modified. However, Kar3, a minus-end directed kinesin, transports unattached kinetochores back to the spindle pole body. Here, we propose that Kip3 is the kinesin that moves kinetochores towards the plus ends of microtubules, similar to CENP-E in mammalian cells.

1.1.2 The microtubule dynamics assay

Currently, methods to observe single kinetochores transported along single microtubules are limited. An ideal assay would enable tracking of single intact kinetochores on microtubules assembled from tubulin isolated from the same species

as those kinetochores; ideally a species with robust genetics so mutants could be used, and an assay that utilizes the full complexity of a cell. A cell-free system combines the full biochemical complexity of a cell with the experimental control provided by *in vitro* experiments. In this study, we investigated mitotic regulation of kinetochore-microtubule attachments and dynamics using a reconstitution system that employs cell cycle arrested extracts from the genetically tractable organism *Saccharomyces cerevisiae* (Bergman *et al.*, 2018).

To investigate the mechanism of kinetochore-microtubule attachment at metaphase, we sought to visualize single kinetochores on single microtubules. For these studies we employed a reconstitution assay wherein cell-cycle arrested whole cell yeast lysate was used to study regulation of microtubule dynamics (Bergman *et al.*, 2018) (Figure 1.2a). Using this assay, we asked whether kinetochores and their dynamics could be observed by TIRF microscopy. Fluorescently tagged kinetochore proteins from each of the major kinetochore sub-complexes were expressed at endogenous levels in strain backgrounds that also expressed fluorescently tagged alpha-tubulin (Tub1) and a temperature-sensitive allele (*cdc23-1*) of the gene that encodes a subunit of the anaphase-promoting complex, to arrest cells in metaphase at the non-permissive temperature (Irniger *et al.*, 1995). The proteins we chose to tag spanned the entirety of the kinetochore (Figure 1.2b) enabling us to track kinetochore dynamics over time (Figure 1.2c), including quantifications of their dynamics via kymographs (Figure 1.2d).

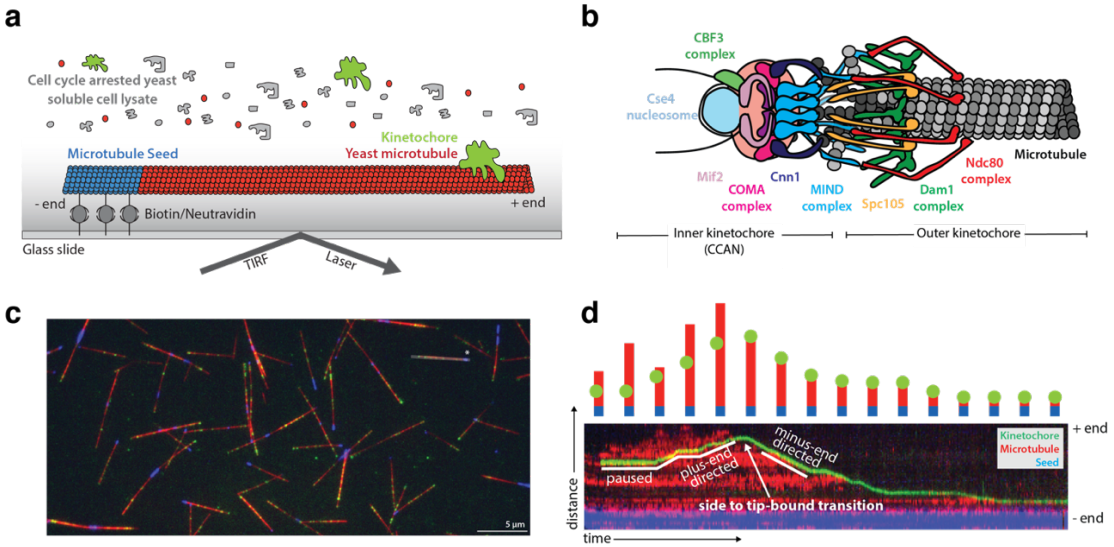

Figure 1.2 The microtubule dynamics assay. (a) A schematic of the microtubule dynamics assay where stabilized microtubule seeds (blue) are adhered to a glass coverslip through a biotin/neutravidin linkage. From the cell cycle arrest yeast soluble lysate, yeast tubulin (red) assembles into microtubules in which native kinetochores and microtubule associated proteins can bind (green). (b) A schematic of the budding yeast kinetochore with its major sub-complexes shown in different colors. The kinetochore is composed of inner kinetochore proteins such as the Cse4 nucleosome and the CBF3 complex, that bind to DNA, and outer kinetochore proteins such as the Ndc80 and Dam1 complex, that bind to the microtubule. (c) A representative image from the microtubule dynamics assay where seeds are blue, yeast microtubules are red, and kinetochores are in green. From these movies we can draw a line along the length of microtubule (asterisk*) to generate kymographs (d) Schematic of a typical kymograph representing a dynamic kinetochore on a microtubule. Time (min) is on the x-axis and distance (µm) is on the y-axis. Above the kymograph is a cartoon depiction explaining how the kymograph shows three-dimensional data in two-dimensional space. In both the kymograph and cartoon, the yeast microtubule is red, the kinetochore is green, and the porcine microtubule seed is blue.

1.2 Results and discussion

1.2.1 Outer kinetochore proteins are dynamic on microtubules

To begin, we tagged two outer kinetochore proteins known to bind to microtubules, Ndc80 (Cheeseman *et al.*, 2006; Wei, Al-Bassam and Harrison, 2007) and the Ask1 subunit of the Dam1 complex (Miranda *et al.*, 2005; Westermann *et al.*, 2005; Jenni and Harrison, 2018). Ndc80 and Ask1 kinetochore signals appeared on the microtubule surface (Figure 1.3a) and moved processively at an average rate of 0.56 μm/min toward the plus end of the microtubule (Figure 1.3b). Upon reaching the tip of the microtubule, Ndc80 and Ask1 appeared to transition irreversibly from lateral to end-on attachment. This end-on binding was then followed by microtubule depolymerization where Ndc80 and Ask1 tracked the depolymerizing microtubule end. The mean microtubule depolymerization rate also slowed from 0.82 μm/min (Bergman *et al.*, 2018) to an average of 0.4 μm/min upon kinetochore binding to the microtubule tip (Figure 1.3b). After depolymerization onset, the microtubule was never observed to resume growth. Additionally, kinetochore proteins rarely, if ever, detached from the microtubule, either while bound laterally or to the microtubule tip. The directional switch of bound kinetochores was striking, as reflected in the dynamics of these kinetochore proteins and the percent of time the associated microtubules spent in the growing versus shrinking phase (Figure 1.3c). While laterally bound, kinetochores only move towards the plus end of the microtubule. When the kinetochore transitions from lateral to end-on attachment, the kinetochore only tracks the depolymerizing end of the microtubule and thus moves toward the minus-end of the microtubule.

In addition to the Ask1 movement that is the same as the Ndc80 movement: laterally along the MT toward the plus end mentioned above, we also observed a distinct Ask1 population that showed a unique behavior compared to other proteins assayed (Figure 1.3a). This Ask1 population was characterized by a very low intensity and diffuse signal, which briefly associated with and moved randomly along the microtubule. The signal to noise ratio was high and it moved faster than our sampling rate. For these reasons, we did not investigate this Ask1 signal further. However, this observation potentially provides insight into Dam1 complex ring assembly and function on the microtubule (Gestaut *et al.*, 2008; Grishchuk *et al.*, 2008).

1.2.2 Inner kinetochore proteins are also dynamic on microtubules

We next tagged and assayed additional kinetochore proteins from the inner and middle kinetochore regions to determine their behaviors and to begin to assess whether all of the kinetochore proteins we observed associated with microtubules as intact kinetochore-like complexes. These additional labeled proteins included: Spc105, Mtw1 (MIND complex) Cnn1, Okp1 (COMA complex), Mif2, Ctf3 (CBF3 complex), and Cse4 (a centromeric histone variant) (Westermann, Drubin and Barnes, 2007; Biggins *et al.*, 2013) (Figure 1.3.a-c). Strikingly, for each kinetochore protein analyzed, we observed dynamics similar to those we observed for Ask1 and Ndc80. Two proteins, Mif2 and Cse4, moved at only 67-75% of the velocity of the others on the microtubule lattice. One possible explanation for the slower velocities of these two proteins is that their GFP protein tags

might affect their function; but since these two proteins colocalize with other kinetochore proteins in lysate from dual-labeled strains (Figure 1.4a), we conclude that all of the proteins examined are present in common complexes. Overall, these seven middle and inner kinetochore proteins have no known microtubule binding capabilities, implying that the kinetochore signals that we observed might represent intact or nearly intact kinetochores on microtubules in our assay.

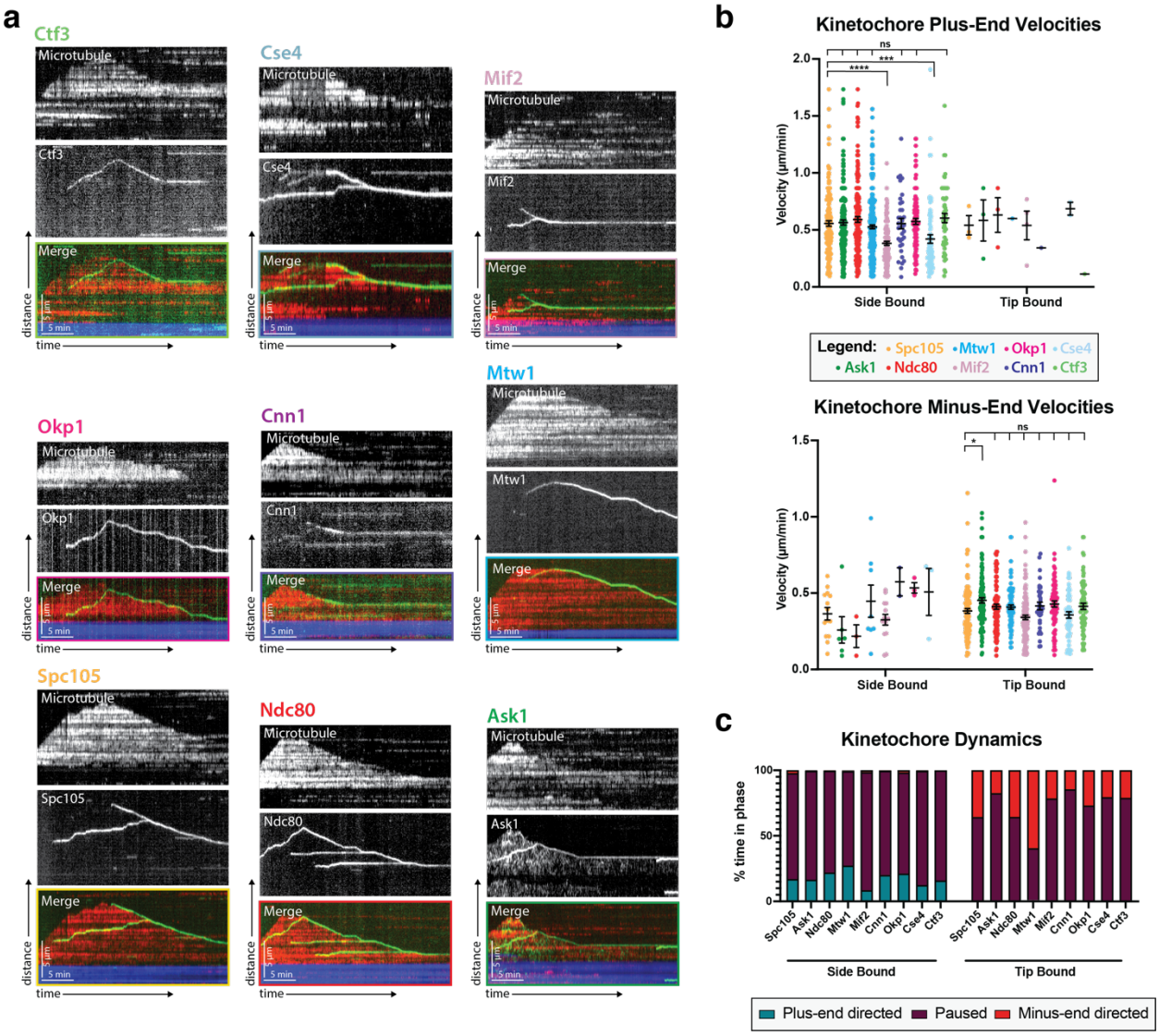

Figure 1.3 Kinetochore reconstitution and dynamics on the microtubule. (a) Reconstituted kinetochore proteins associated with yeast microtubules. Representative kymographs of kinetochore proteins from each sub-complex are shown. Time is on the x-axis and distance is on the y-axis (scale bars are 5 min and 5 μm, respectively). Kinetochore proteins are green and yeast microtubules are red. The porcine seed is blue. Each of the proteins assayed displays similar dynamics: moving toward the microtubule plus end when bound to the microtubule lateral surface. When the kinetochore proteins reach the plus end of the microtubule, they appear to convert from lateral to end-on attachment, which is often followed by microtubule depolymerization with the kinetochore remaining associated with the plus end. The microtubules were never observed to grow again following the depolymerization events in which a kinetochore protein was attached end-on. (b) Quantification of velocities and dynamics of kinetochores bound to microtubules. Kinetochores bound to the sides of microtubules move toward the microtubule plus end at an average velocity of 0.56

μm/minute. There were negligible minus-end directed movements when the kinetochore was side bound. When the kinetochores were associated with the microtubule tips, they tracked the microtubule tips as they depolymerized, moving at an average velocity of 0.4 μm/minute. There were also negligible plus-end directed movements when the kinetochore was bound to the tip. Each data point in the graph is the average velocity of one kinetochore. The error bars are the mean and standard error of the mean from 4 replicate trials of two biological replicates. Statistical analysis was done by a Kruskal-Wallis test where **** is $P < 0.0001$, *** is $P = 0.0003$, and * is $P = 0.0132$. For the different kinetochore proteins: from Spc105 in order in the figure to Ctf3, N = 128, 155, 116, 102, 174, 56, 77, 59, 87 proteins tracked, respectively. (c) When the kinetochore is bound to the side of a microtubule, about ~30% of its time it is in plus-end directed motion and the remaining ~70% of the time it is paused (not moving). Kinetochores associated with plus ends spend ~40% of the time moving toward the minus-end and ~60% of the time paused.

1.2.3 Kinetochore proteins from different sub-complexes move together on microtubules

The observation that inner kinetochore proteins (such as Cse4) which do not physically bind to microtubules, are in fact able to bind to and translocate on microtubules in our assay provided evidence that these kinetochore proteins were not alone or in small sub-complexes, but, in fact, were part of complete or nearly complete kinetochores. To explore this possibility further, we turned to dual-color imaging of kinetochore protein pairs and colocalization analyses. Due to its well-documented and canonical microtubule binding abilities, Ndc80 was chosen as a fiducial marker to which the localization of other kinetochore proteins was compared (Ciferri, Musacchio and Petrovic, 2007). One possibility was that proteins that reside further away from the Ndc80 complex would colocalize less frequently in our assay than proteins located closer to or adjacent to the Ndc80 complex. On the contrary, when imaging different kinetochore proteins together with Ndc80, we, in fact, saw colocalization independent of that kinetochore protein's proximity to Ndc80 within the kinetochore. Additionally, when using Mtw1, a more "central" kinetochore protein, as a fiducial marker, we still observed colocalization between kinetochore proteins (Figure 1.4). These data indicate that the characterized movements of single tagged kinetochore proteins in this assay likely represents entire kinetochore complexes.

In our assay, the mScarlet-I fluorophore used to tag proteins blinked on and off (Klementieva *et al.*, 2017). Other red fluorescent protein tags tested, including mScarlet, TagRFP-T, and mRuby2, also blinked and/or bleached rapidly. From our single protein tagging (with GFP) experiments (Figure 1.3), we knew that Ndc80 and Mtw1 never disassociated from microtubules to which they were bound. Therefore, the patchy signal we saw with mScarlet-I fluorophore (Figure 1.4a) was likely a result of our red fluorescent protein blinking on and off. This also meant that it was nearly impossible to draw any conclusions about kinetochore assembly on the microtubule at any single point in time (i.e., during lateral movement or the transition from lateral to end-on binding). But the colocalization of entire tracks over time in the kymographs (Figure 1.4b), even with one reporter signal blinking, indicated that a multi-complex of kinetochore proteins was observed on microtubules in our assay.

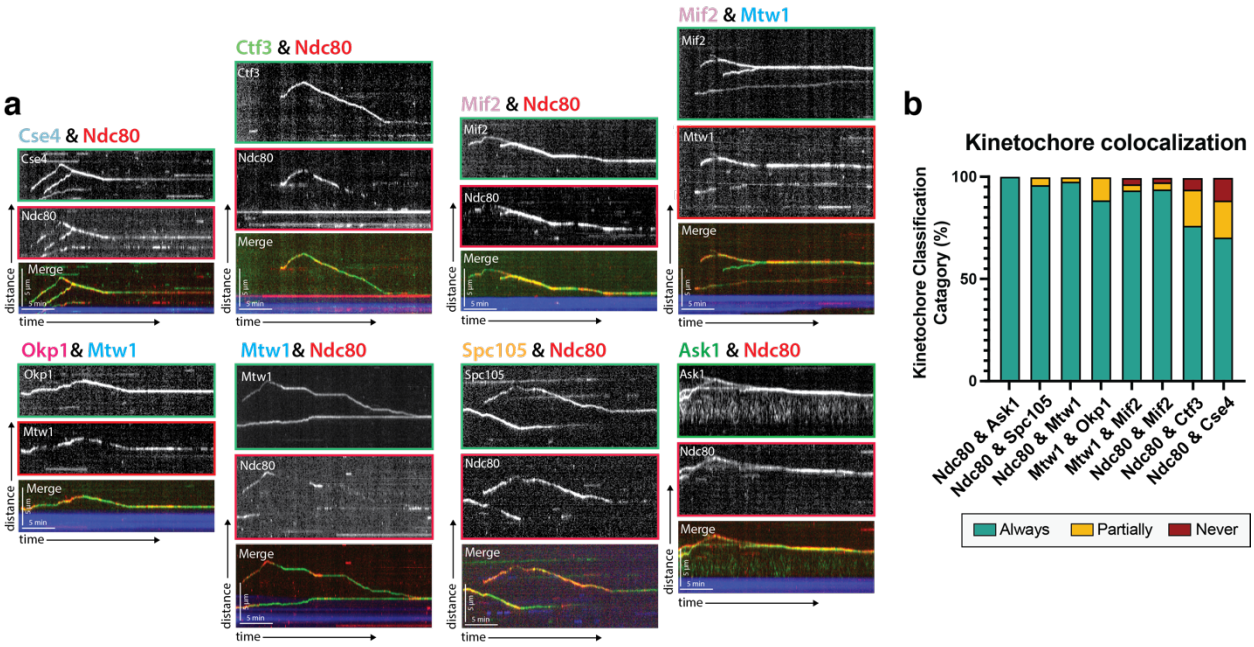

Figure 1.4 Protein composition of reconstituted kinetochores. (a) Different pairwise combinations of kinetochore sub-complex proteins colocalize, establishing that the kinetochore spots observed by fluorescence microscopy are multi-protein, multi-subcomplex assemblies. Representative kymographs from each strain expressing a different pair-wise combination of tagged kinetochore proteins are shown. Time is on the x-axis and distance is on the y-axis (scale bars are 5 min and 5 μm, respectively). Ndc80 was used as the common reference marker for multiple pairwise combinations. Additionally, Mtw1 was used in some pairwise combinations to show that multiple sub-complexes are present in the same kinetochore. The tracks of these colocalized proteins follow similar dynamics as in Figure 1, where they move processively toward the microtubule plus end. At a certain point, they reach the plus end and motility becomes minus-end directed concomitant with the onset of microtubule disassembly (note that the microtubules are not visualized due to the inability to measure 4 colors, and the assumption is that this directional switch in kinetochore protein motility corresponds to microtubule depolymerization onset shown in Figure 1.3). (b) Quantification of kinetochore colocalization for each pair-wise protein combination. Kinetochore tracks were grouped into three distinct pools and counted. These categories were “always” colocalized (blue), “partially” colocalized (yellow), or “never” colocalized (red). For partially colocalized tracks, the mScarlet signal initially appears alone, but a GFP signal appears on it and stays colocalized for the remainder of the movie. For the different kinetochore protein pairs in order in the figure: from Ndc80 & Ask1 to Ndc80 & Cse4, N = 70, 49, 42, 52, 120, 81, 116, 97 tracks categorized, respectively, from two experimental replicates.

1.2.4 Cryo-correlative light microscopy and electron tomography provides evidence that the reconstituted kinetochores are largely intact

Cryo-electron tomography (cryo-ET) is a powerful method for studying the structural organization of multi-protein complexes in their fully hydrated, native state (Schur, 2019). A challenge in cryo-ET is to relate specific protein localization to the complex structural information that can be obtained with this method. To overcome this challenge and to test whether the kinetochore proteins in our reconstitution assay are indeed part of higher-order kinetochore assemblies, we established a cryo-correlative light microscopy and electron tomography procedure. In brief, samples were prepared from yeast cell lysates with GFP-labeled Spc105 and mRuby2-labeled Tub1 incubated with far-red MT seeds in a similar fashion to the TIRF assay (see Materials and Methods for details). Samples were vitrified and first imaged by cryo-fluorescence light microscopy to identify regions of interest for cryo-ET data collection (Figure 1.5a, c). The

holey carbon film generated some fluorescent background in the GFP channel, but we could detect clear Spc105-GFP foci. These foci were then targeted for cryo-ET imaging. Large protein complexes associated with the lateral surface and the tip of individual microtubules were clearly visible in tomograms of these regions. These approximately 100 nm long complexes are reminiscent of kinetochore particles assembled from purified yeast components (Gonen *et al.*, 2012) (Figure 1.5b, d). Furthermore, our tomography data revealed electron densities that likely correspond to the Dam1 ring and the Ndc80 and MIND sub-complexes (Westermann *et al.*, 2005; Jenni and Harrison, 2018; Ng *et al.*, 2019) (Figure 1.5b, d). In combination with the co-localization data from the TIRF assay, our tomography data reinforces the conclusion that multi-protein kinetochore particles were present on yeast microtubules in our reconstitution cell lysate assays.

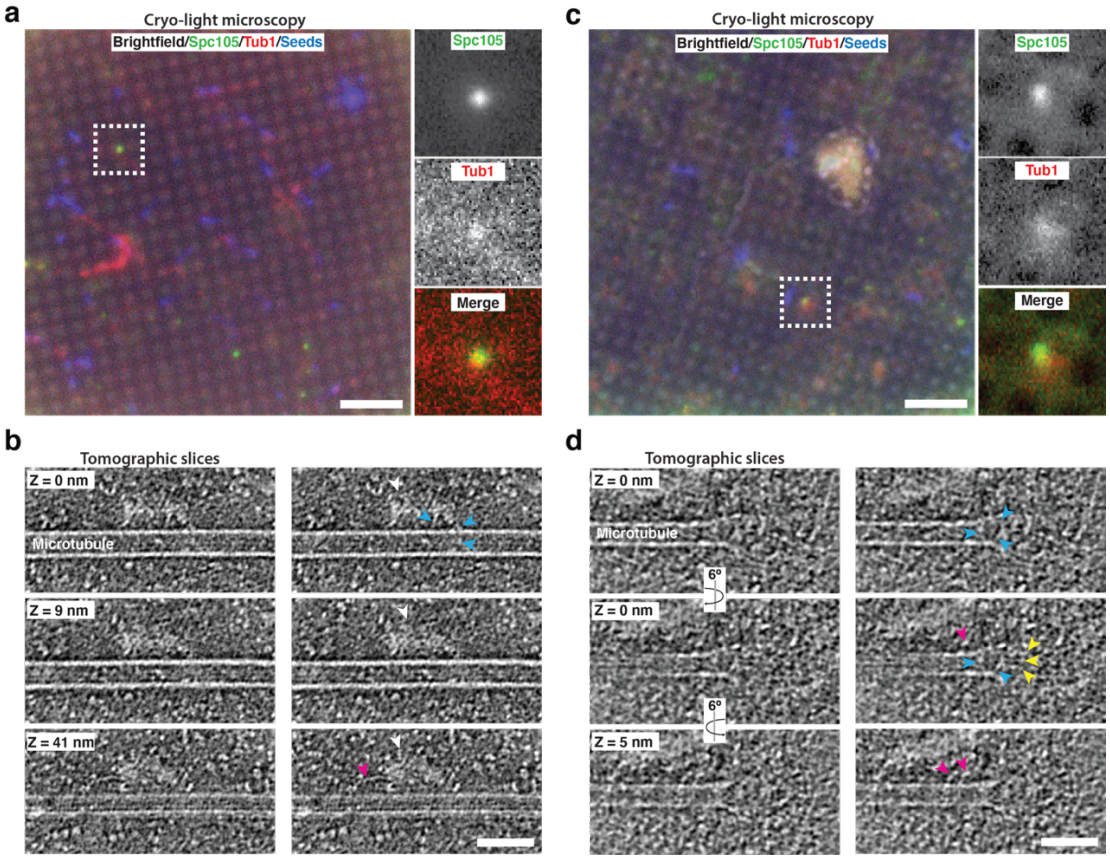

Figure 1.5 Cryo-correlative light microscopy and electron tomography shows microtubule-associated intact kinetochore complexes. (a),(c) Overlay of brightfield and fluorescent channel cryo-light micrographs showing Spc105-GFP in green, mRuby-Tub1 in red and microtubule seeds in blue. The brightfield channel highlights the holey carbon film pattern. Insets show 2.7x magnified views of boxed regions. (b) Slices of tomogram recorded in the region of the highlighted Spc105 focus in (a) at Z-positions relative to the top slice. Slices show a kinetochore bound to the lateral surface of a microtubule. The largest part of the kinetochore appears as an electron-dense proteinaceous cloud similar to what has been reported for purified yeast kinetochores (white arrowheads; Gonen et al., 2012). A ring-like density (blue arrowheads) and a rod-like density (pink arrowheads), potentially representing Dam1 and Ndc80 sub-complexes, respectively, extend from the cloud-like density. (d) Slices of tomogram recorded in the region of the highlighted Spc105 focus in (c) at Z-positions relative to the top slice, showing a kinetochore complex bound to the end of a microtubule. Arrowheads point at a ring-like (blue) and rod-like (pink) density similar to the ones observed in (b) Additional rod-like extensions (yellow arrowheads) might represent the MIND complex. Right columns in (b,d) show the same images as in the left column, but protein densities are colored to match the arrows. Scale bars, 10 µm in (a,c) 60 nm in (b,d).

1.2.5 Kip3 is involved in kinetochore movement toward the microtubule plus end

After establishing that the kinetochore protein signals observed in our reconstitution assay represented intact kinetochore complexes, we began to probe the mechanism of the plus-end directed kinetochore movement. We postulated that the movement was driven by a kinesin motor protein. In budding yeast, there are only 5 kinesins, Kip2, Kip3, Cin8, Kip1, and Kar3 (Cottingham *et al.*, 1999). To test the possibility that one of these motors was involved in kinetochore movement along microtubules in our assay, we systematically deleted each kinesin and asked whether kinetochore motility was impaired.

Upon deleting the genes encoding each of these motors, we found that only the highly processive plus-end directed kinesin-8, Kip3, was necessary for plus-end directed motility of the kinetochores. Specifically, 77% of laterally bound kinetochores moved in Kip3+ lysates compared to only 28% in *kip3Δ* lysates. Moreover, those laterally bound kinetochores that did move in *kip3Δ* lysates spent significantly less time moving toward the microtubule plus end compared to wild-type, and their run lengths were about half as far as those in Kip3+ lysates (0.46 μm vs 0.73 μm) (Figure 1.6b, c). Interestingly, although less frequent and covering shorter distances, kinetochore movements in *kip3Δ* lysates had the same velocity as the more frequent and longer movements observed in Kip3+ lysates, moving at 0.47 μm/min (Figure 1.6d) (see Conclusion 1.3).

Because the kinetochore movements in the *kip3Δ* lysate were relatively infrequent and covered short distances, only 5.7% of laterally bound kinetochores reached the plus end, compared to 28.1% in Kip3+ lysates. As in the Kip3+ lysates, when the kinetochore in the *kip3Δ* lysates was bound to the tip of the microtubule, depolymerization with the kinetochore tracking the microtubule plus end did occur. However, in this *kip3Δ* case, the microtubule plus ends with tip-bound kinetochores spent a significantly lower percentage of the time depolymerizing compared to what we observed in Kip3+ lysates (Figure 1.6b). This observation is consistent with a role for Kip3 in kinetochore-induced microtubule depolymerization (Gupta *et al.*, 2006).

Although Kip3 is required for kinetochore motility, whether kinetochores that were assembled and bound to the lateral surface of microtubules in the absence of the kinesin could be induced to move processively by retroactive addition of Kip3 was not clear. It was possible that an important binding surface for the kinesin or its cargo would only be accessible when the kinetochore was partially assembled or unattached to microtubules. Therefore we tested whether providing a source of wild-type Kip3 to stationary kinetochores on microtubules assembled in *kip3Δ* lysates would enable those kinetochores to start to move. After observing immobile kinetochores on microtubules assembled in *kip3Δ* lysates for 10 minutes, lysate from a Kip3+ strain was added to the chamber. Immediately, these same stationary kinetochores began to move processively toward microtubule plus ends, establishing that Kip3 acts on previously microtubule-bound kinetochores (Figure 1.6e). Specifically, 53.7% of the 54 immobile, laterally bound kinetochores in the *kip3Δ* lysates became motile after Kip3+ lysate was added. Therefore, kinetochores assembled in the absence of Kip3 were able to bind to

microtubules, but required the subsequent addition of Kip3 and/or its other binding partners to translocate along the lateral surface of microtubules.

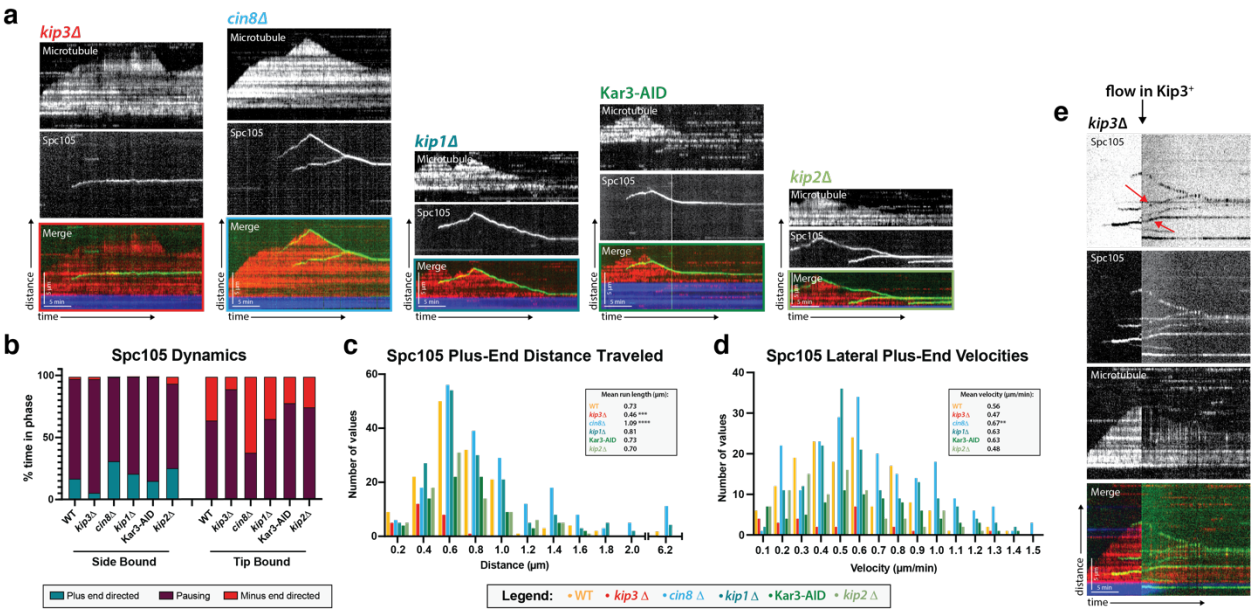

Figure 1.6 Kip3, a kinesin-8 motor, is required for plus-end directed movement of the kinetochore on the microtubule lattice. (a) Genes encoding each of the five yeast kinesins were individually deleted (or the proteins degraded using a degron tag) and kinetochore dynamics on microtubules were assayed. Only Kip3, a highly processive kinesin-8, was required for kinetochore movement toward the microtubule plus end. Representative kymographs are shown with time on the x-axis and distance on the y-axis (scale bars are 5 min and 5μm, respectively). The kinetochore (Spc105) is shown in green and the microtubule is shown in red. The microtubule seed (at the minus-end of the growing red yeast microtubule) is shown in blue. (b) Quantification of dynamics over time shows that kinetochores in the kip3Δ strain spend the majority of the time paused, moving toward the plus end only ~5% of the time compared to ~30% for wild-type. (c) Run lengths and the number of runs the kinetochore made on the lattice toward the plus end were decreased in the kip3Δ strain. Run lengths were about half of wild-type, 0.46 μm vs 0.73 μm. The number of runs was also decreased to about 25% of the wild-type number of runs. Statistical analysis was done by a Kruskal-Wallis test where *** is P = 0.0001 and **** is P <0.0001. (d) Laterally bound kinetochores velocities are unchanged when moving in the plus end direction in a kip3Δ lysate. Statistical analysis was done using a Kruskal-Wallis test where ** is P = 0.0047. (b-d) Quantification is from 4 replicate trials of two biological replicates. For each strain from WT to kip2Δ lysate in the order listed, N = 128, 70, 129, 144, 103, 154 Spc105 proteins tracked. (e) Adding back a source of Kip3 to a lysate from a kip3Δ strain restores plus end-directed kinetochore movement. In lysates lacking Kip3, Spc105 (green) was immobile on the microtubule (red) surface. When Kip3+ lysate was added, the same, previously immobile, kinetochores started to translocate towards the microtubule plus ends (marked with red arrows).

1.2.6 Processive Kip3 transiently encounters slower moving kinetochores

We next set out to investigate the molecular mechanism by which Kip3 facilitates kinetochore plus end movement. To start, we asked whether we could observe Kip3 stably associated with moving kinetochores. To achieve this goal, we carried out dual-color imaging of the kinetochore (Spc105) and each of the motors assayed in the motor deletion screen described above. We observed Cin8 and Kip1 coming on and off the microtubule lattice stochastically at a high frequency, but they were not motile in our assay (Figure 1.7a). Kar3 was rarely observed on the microtubule (Figure 1.7a). For these three motors, anti-parallel or parallel bundled microtubules might be necessary to

observe their previously reported activities in lysate (Su *et al.*, 2013; Hepperla *et al.*, 2014).

Of all the motors assayed, only Kip3 and Kip2 moved processively on the microtubule lattice (Figure 1.7a). However, kinetochore motility was only disrupted in *kip3Δ* lysates, not in *kip2Δ* lysates (Figure 1.6a-d). Therefore, processive motor movement towards the plus end alone is not sufficient to facilitate kinetochore movement along a microtubule. Kinetochore plus-end directed movement is dependent on Kip3 activity specifically. However, neither motor showed persistent colocalization with the kinetochores. The dual color tagging of Kip3 and Spc105 showed that there were brief moments of kinetochore movement where Kip3 signal was observed running over or through the kinetochore signal. Kip3 also moved much faster than either the speed of the kinetochore or the polymerization of the microtubule. However, Kip3 density on the microtubule was also very high and the bright signal might have obscured any Kip3 associated stably with kinetochores (see Conclusion 1.3).

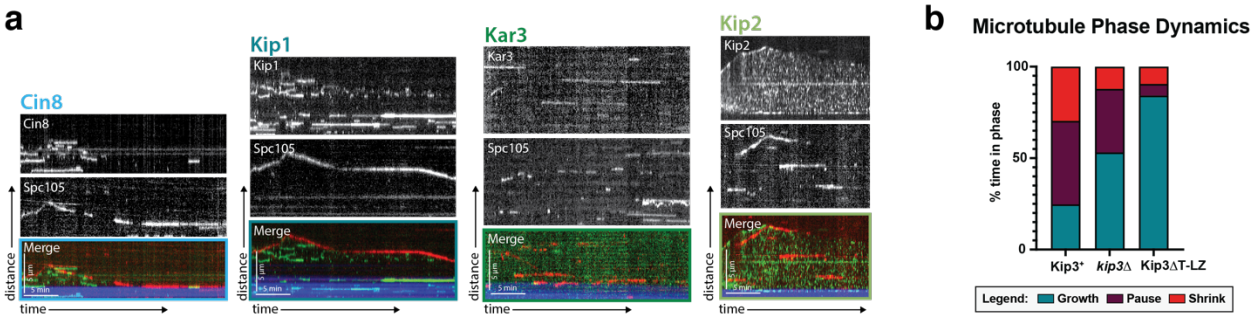

Figure 1.7 Kinetochores do no colocalize with the other four kinesins and Kip3's effect on microtubule dynamics. (a) Dual color tagging of the kinetochore protein Spc105 and each of the five kinesins shows no clear colocalization. Representative kymographs are shown with the Spc105 in red and the kinesin motor proteins in green. The microtubule seed (minus-end) is in blue. (b) Across each of the three Kip3 conditions: wild-type, kip3Δ, and Kip3ΔT-LZ, the time the microtubule spent growing, shrinking, and paused changes. Wild-type Kip3 is the most dynamic, spending almost equal time in all three phases. The kip3Δ strain has an increased time spent paused and growing, while the Kip3ΔT-LZ strain spends the most time growing, rarely pausing or shrinking.

1.2.7 Kip3's tail domain is not needed for kinetochore motility, but Kip3's ability to attenuate microtubule dynamics is needed for kinetochores to reach the microtubule plus end

Comparison of *in vitro* and *in vivo* phenotypes of different Kip3 mutants provide insights into the role of Kip3 in establishment of end-on attachments. In cells, knocking out the gene encoding Kip3 results in metaphase kinetochores that stay along the axis of the spindle, but are no longer focused into two discrete foci (Figure 5a-b) (Tytell and Sorger, 2006; Wargacki *et al.*, 2010; Su *et al.*, 2011). This declustered kinetochore phenotype has been proposed to be a result of improper spindle assembly and/or defective kinetochore-microtubule attachment (Shimogawa *et al.*, 2010). Of interest to us was a Kip3 mutant, Kip3ΔT-LZ, that shows a declustered kinetochore phenotype *in vivo* (Figure 1.8a-b) (Su *et al.*, 2011). In Kip3ΔT-LZ, the putative cargo-binding tail was truncated and replaced with a leucine zipper domain from Gcn4 transcription factor to restore dimerization of the motor heads (Su *et al.*, 2011). Because the declustered chromosome phenotype *in vivo* is believed to be due to defects in kinetochore attachment, we

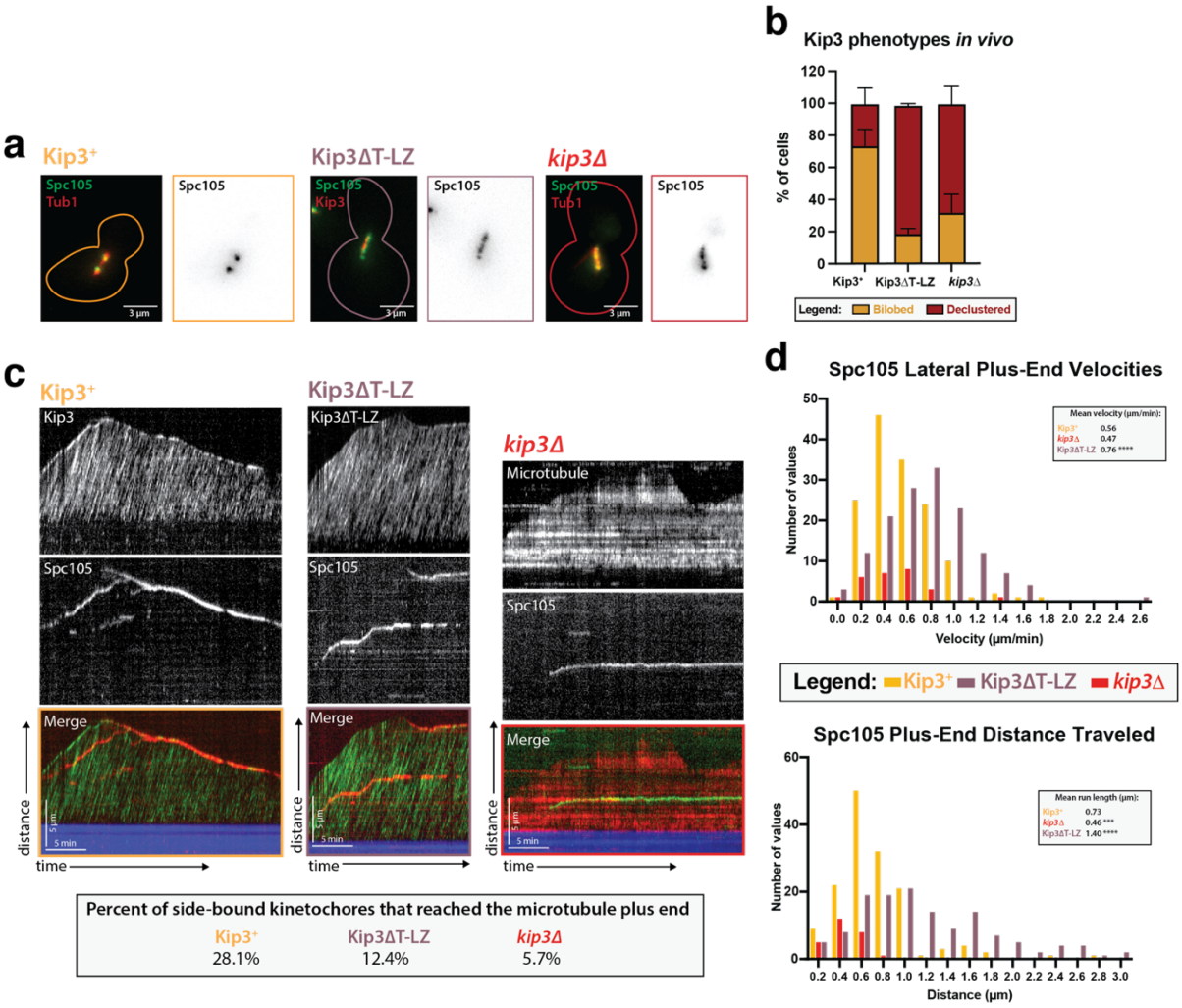

Figure 1.8 Kip3's motor activity, but not its depolymerase tail domain, is necessary for processive plus end-directed kinetochore movement. (a) Metaphase cells with either wild-type Kip3, kip3Δ, or kip3ΔT-LZ alleles imaged in a cdc23-1 strain expressing Spc105-GFP (green), mRuby-Tub1 or Kip3 (red). Note that the cells were not shifted to non-permissive temperature and were not arrested for imaging. Images are a maximum Z-projection of a 5µm stack of 0.2µm slices. (b) Quantification of the declustered kinetochore phenotype is shown as a bar graph for spindles that were ~2-3 µm in length. Cells were classified as "bi-lobed" by a line scan showing two distinct peaks. The "declustered" phenotype included all line scans that did not show two peaks (line scans not shown). Two replicates were performed, each with n = 50 cells. Error bars are standard error of the mean. (c) Representative kymographs of Spc105 motility in wild-type, kip3ΔT-LZ, and kip3Δ lysates. Dual color tagging of wild-type Kip3 and Spc105 showed no clear colocalization between the kinetochore (red) and Kip3 (green). Kip3 is highly processive, moving much faster than the kinetochore. A Kip3 mutant containing a deletion in the tail region (Kip3ΔT-LZ, green) with the kinetochore (red) was still processive along the microtubule. The Kip3ΔT-LZ mutant showed robust processivity but it did not accumulate on microtubule plus ends and depolymerization events were fewer than in Kip3+ lysates, as shown in previously published literature. Lastly, a representative kymograph for kip3Δ lysate shows immobile Spc105 (green) on microtubules (red). (d) Histograms of Spc105 velocities and average run length when laterally bound and moving toward the microtubule plus ends. The number of values is shown on the y-axis and velocity/distance traveled on the x-axis, binned every 0.2 units. The mean velocity of wild-type Kip3 protein and Kip3ΔT-LZ protein is 0.55 µm/min and 0.76 µm/min, respectively. The average run length also increased from 0.73 µm to 1.4 µm. The mean Spc105 velocity in kip3Δ lysates was unchanged compared to wild-type, but the number of runs was reduced to ~25% of wild-type. The average length decrease in kip3Δ was reduced from 0.73 µm to 0.45 µm. The mean is from 2 replicate trials of one biological replicate. Statistical analysis was done using a Kruskal-Wallis test where *** P = 0.0006 and **** P <0.0001. For lysates from each strain, as listed from WT to Kip3ΔT-LZ, N =128, 70, 81 kinetochores tracked.

hypothesized that, in our *in vitro* assay, we would observe laterally attached kinetochores in *kip3ΔT-LZ* lysates that do not become properly end-bound, similar to what we observed in *kip3Δ* lysates. Strikingly, in *kip3ΔT-LZ* lysates, kinetochores still moved processively toward the plus end of microtubules. In fact, deleting the tail domain increased the velocity and the average run length of the kinetochore on the lattice of the microtubule (Figure 1.8d). In Kip3+ versus *kip3ΔT-LZ* lysate, the laterally bound plus end velocity increased from 0.56 μm/min to 0.76 μm/min and the average run length increased from 0.56 μm/min to 1.4 μm/min (Figure 1.8d).

As previously reported, the Kip3ΔT-LZ mutant protein did not accumulate on the plus ends of microtubules and it was unable to destabilize their plus ends and cause depolymerization (Su *et al.*, 2011) (Figure 1.7b). Similarly, in a *kip3Δ* lysate, there was also altered microtubule dynamics, specifically a diminished catastrophe frequency (Bergman *et al.*, 2018) (Figure 1.7b). Because of the reduced microtubule catastrophe frequency, we observed that in *kip3ΔT-LZ* lysates the kinetochore rarely reached the plus ends of polymerizing microtubules, despite its faster velocity. Moreover, compared to the Kip3+ lysates wherein 28.1% of kinetochores completed travel to the microtubule plus end, only 12.4% of kinetochores made it to microtubule plus ends in *kip3ΔT-LZ* lysates. The decreased kinetochore movement to microtubule plus ends was even more dramatic in *kip3Δ* lysates, where only 5.7% of kinetochores reached the plus end (Figure 1.8c). These results indicate that the Kip3 tail domain is not required for kinetochore movement along microtubules, but it is required for kinetochores to reach the plus end. We conclude thatKip3's dual functions are: (1) attenuating microtubule growth, and (2) enabling movement of kinetochores processively on the lattice to allow end-on attachments to be made (see Conclusion 1.3).

1.3 Conclusion

Here we present a novel assay to follow kinetochore movement on microtubules in a cell free yeast system. We demonstrate that this assay allows individual kinetochores to be visualized while they are interacting with single microtubules. We observed kinetochore binding to microtubules, movement toward the microtubule plus end along the lattice, transition from side- to end-on attachment, apparently inducing depolymerization, and tracking of the depolymerizing end. Development of this kinetochore assay was achieved by adopting a previously established yeast extract system that allows analysis of dynamics of single yeast microtubules assembled in the presence of the full complement of yeast proteins at defined cell cycle stages (Bergman *et al.*, 2018). This assay involves native yeast proteins and allows us to combine the control over conditions provided by complementary powers of biochemistry and genetics to establish functions. One limitation of this system that we hope to address in the future is that molecules that are normally compartmentalized to either the nucleus or the cytoplasm are mixed. We propose a model wherein kinetochores move to the microtubule plus ends powered by the budding yeast kinesin-8, Kip3. When kinetochores reach the microtubule plus ends, their attachments are converted to end-on attachments, at which point microtubule disassembly ensues (Figure 1.9).

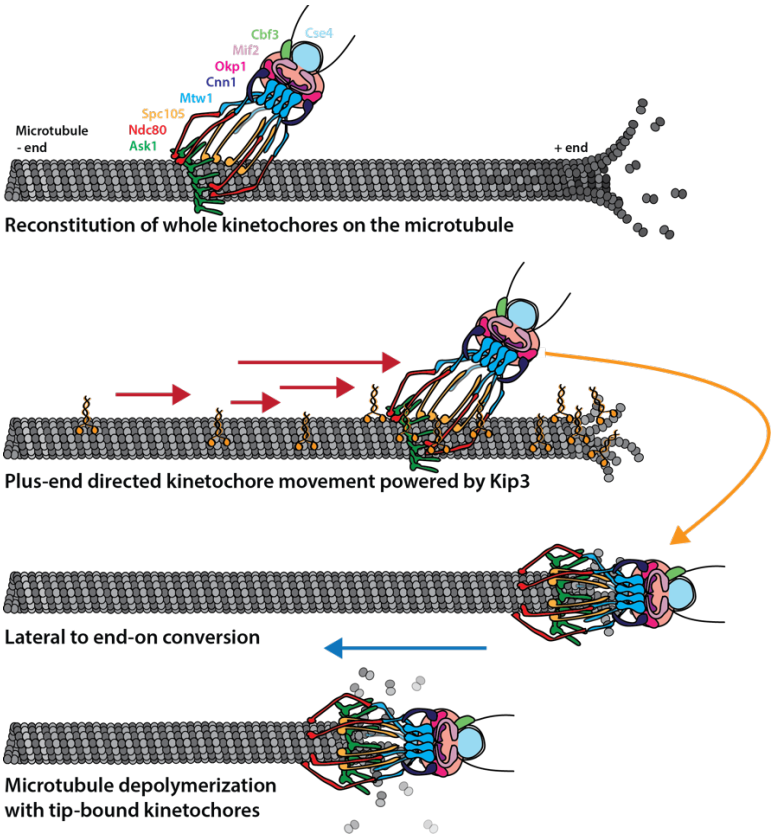

Figure 1.9 Cartoon model of reconstituted kinetochore dynamics on the microtubule. Yeast kinetochores reconstituted binding with individual yeast microtubules in a yeast protein extract. These laterally-bound kinetochores travel in a directional manner to the plus end of the microtubule, powered by the kinesin-8, Kip3. Upon reaching the end of the microtubule, the kinetochore transitions to end-on attachment. Establishment of this end-on attachment coincides with onset of microtubule depolymerization and the end-bound kinetochore preventing the microtubule from elongating again.

Using both TIRF microscopy and cryo-electron tomography, we verified successful reconstitution of intact, microtubule-bound kinetochores. We observed nine different kinetochore proteins, spanning five kinetochore sub-complexes, and found that they all associate with and move along microtubules with similar dynamics (Figure 1a-e). The common behavior of these kinetochore proteins, combined with their colocalization with each other (Figure 1.4), indicated that kinetochore particles that contain multiple subunits from different subcomplexes were observed in the assay. Since our assay does not involve biochemical fractionation steps, and since the lysates retain the relative physiological concentration and ratio of soluble proteins, we were able to preserve the natural kinetochore composition (Biggins *et al.*, 2013). Most importantly, by using cryo-correlative light-microscopy and electron tomography, we were able to directly visualize kinetochores bound to both the sides and ends of microtubules and found that their structures closely resemble negatively stained yeast kinetochores observed in earlier studies (Gonen *et al.*, 2012). In both side- and end-bound arrangements, these kinetochore complexes included rod-like and ring-like structures that most likely are the Ndc80 complex and the Dam1 complex, respectively (Figure 1.5a-d) (Westermann *et al.*, 2005; Gonen *et al.*, 2012; Jenni and Harrison, 2018; Ng *et*

al., 2019). Taken together, these observations establish that we were able to recapitulate dynamic kinetochore-microtubule binding in an *in vitro* reconstitution assay.

The ability to visualize individual kinetochores associated with single microtubules made possible quantitative analysis of their dynamics along microtubules, which mimicked kinetochore behavior observed in spindles *in vivo* (Maiato *et al.*, 2017). Kinetochores that bind to the side of the microtubule lattice move processively towards the plus end. Upon reaching the microtubule end, kinetochores convert their attachment to an end-bound conformation. During their conversion from lateral- to end-on attachment, and while bound to the microtubule end, kinetochores remain stably attached to the microtubule. Once bound to the microtubule ends, kinetochores track the tip of the depolymerizing microtubule. This transition to stable end-on attachments appeared to block microtubule polymerization and to induce depolymerization at a rate slower than the catastrophe rate for microtubules lacking kinetochores (Bergman *et al.*, 2018) (Figure 1.3a-e). While tension stabilizes kinetochore-microtubule attachments on dynamic microtubules (Akiyoshi *et al.*, 2010), in our presumably tension-less system, there was no observable kinetochore detachment from microtubule plus ends. Differences in kinetochore composition, cell cycle specific post-translational modifications, species-specific tubulin, buffer composition, or the presence of unidentified helper proteins could account for the differences. Notably, end-bound kinetochores do not normally detach from microtubules *in vivo* after attachment has been established during S phase (Tanaka, Stark and Tanaka, 2005). Additionally, in a previous *in vitro* study, chromosomes remained stably associated with depolymerizing microtubule ends (Koshland, Mitchison and Kirschner, 1988). In the future, adapting our assay to include tension across the kinetochore promises to provide insights into how force impacts attachment and motility parameters. In summary, we were able to reconstitute intact kinetochores that associated with microtubule lateral surfaces and then underwent conversion to end-on attachment, which was followed by Anaphase A-like kinetochore-microtubule dynamics, with the kinetochores staying associated with depolymerizing microtubule plus ends.

Strikingly, reconstituted intact kinetochores associated with the lateral surface of dynamic microtubules stably, and they moved exclusively toward the plus end, and in a processive and kinesin-8-dependent manner. This behavior contrasts with the *in vivo* observation of chromosomes binding to the lateral surface of microtubules and moving exclusively toward the minus-end in a Kar3-dependent manner (Tanaka *et al.*, 2005). We speculate that these two distinct and opposite-directed mechanisms both exist in yeast to fulfill different functions. In mammalian cells, dynein has been reported to transport chromosomes captured by astral microtubules toward the centrosome, while chromokinesins are implicated in moving laterally-bound chromosomes in the plus end direction toward the spindle equator to promote amphitelic sister kinetochore attachment (Maiato *et al.*, 2017). We propose that in yeast, minus-end-directed Kar3 may transport chromosomes toward the spindle pole, while Kip3 moves chromosomes toward the equator. These two mechanisms may increase resilience to different stresses. Further studies are required to fully explore how these two mechanisms are employed in normal and stressed conditions.

In our assay, kinetochores reached the plus end via a combination of directed movement and microtubule catastrophe. A role for Kip3, the budding yeast kinesin-8, in the translocation of kinetochores along microtubules is consistent with Kip3's reported *in vivo* colocalization with kinetochores and with its Ndc10-dependent association with centromeric DNA in ChIP assays (Tytell and Sorger, 2006). While our experiments did not show strong colocalization of Kip3 and kinetochores, it is possible that weak transient interactions are what facilitates kinetochore mobility via Kip3 (Figure 1.8c), or that low stoichiometry of Kip3 stably associated with kinetochores made detection impossible against a high background (Figure 1.8c) of free Kip3 molecules on the microtubules. Additionally, quantification of kinetochore velocity on the microtubule lattice showed a wide distribution of rates punctuated by frequent pausing (Figure 1.3d-e). Both of these observations lend themselves to a model in which Kip3 affects kinetochore mobility in a stochastic way, perhaps by binding transiently. By this model, Kip3 sometimes moves the kinetochore in longer, faster runs, while other times, it displaces the kinetochore a short distance. Significantly, another processive microtubule-plus-end directed motor protein, Kip2 (Figure 1.7b), was insufficient to move kinetochores in *kip3Δ* lysates, which diminishes the possibility that non-specific collisions with the motor proteins are driving kinetochore translocation. The plus-end directed kinetochore motility we observed is specifically dependent on a processive Kip3 motor and was not dependent on this kinesin's tail domain. In the absence of the ability to consistently observe direct Kip3 stable association with motile kinetochores, we cannot rule out other mechanisms to explain the Kip3-dependent kinetochore motility that we discovered. Further investigation is required to determine the exact molecular mechanism by which Kip3 mediates plus end-directed kinetochore transport on the microtubule lattice. It is possible, for example, that Kip3 transports an unidentified factor to kinetochores, and that this hypothetical factor mediates kinetochore movement.

We propose that Kip3 has a dual function in facilitating end-on attachment: (1) it induces microtubule catastrophe to allow kinetochores to catch up with elongating microtubule plus ends, and (2) it moves kinetochores to the microtubule plus ends. Kinetochores did not move as frequently, directionally, or as far along microtubules in the *kip3Δ* lysate, but they did move in a highly processive manner in *kip3ΔT-LZ* lysates (Figure 1.8c-d). However, in lysates made from both Kip3 mutants (*kip3Δ* or *kip3ΔT-LZ*), we observed kinetochores that are laterally attached to microtubules, but these kinetochores rarely became end-bound. This observation can be explained if fewer kinetochores make it to the end of the microtubule. Specifically, in *kip3Δ* lysates, the inability to establish end-on attachments is likely largely due to a combination of impaired kinetochore motility and due to the microtubule dynamics being shifted toward more elongation with fewer catastrophes, making it less likely that kinetochores will reach microtubule plus ends (Figure 1.6a-d) (Figure 1.7b). In contrast, in *kip3ΔT-LZ* lysates the kinetochores are highly motile, but they establish end-on attachments less frequently than in wild-type lysates. This result can be explained by the observations that the catastrophe frequency is severely diminished compared to wild-type microtubule dynamics, and that the microtubules mostly elongate faster than the rate of kinetochore

translocation, so the kinetochores are less likely to encounter plus ends (Figure 5c-d) (Figure 1.7b).

It is useful to consider these *in vitro* results in the context of observations of kinetochore behavior in the corresponding mutant cells. In wild-type cells, sister chromatids are clustered in two foci within the metaphase spindle. In contrast, in *kip3Δ* cells metaphase kinetochores are declustered and aligned linearly along the spindle microtubules. This declustered kinetochore phenotype is also seen in *kip3ΔT-LZ* cells (Tytell and Sorger, 2006; Wargacki *et al.*, 2010; Su *et al.*, 2011) (Figure 1.8b). Based on the above *in vitro* and *in vivo* observations, we hypothesize that laterally bound kinetochores are an intermediate on the pathway toward biorientation, and that Kip3 is required for moving laterally attached kinetochores to the plus end of the microtubule during prometaphase. Specifically, we speculate that the previously reported declustered kinetochore phenotype is the result of an increased number of laterally bound kinetochores stalled all along spindle microtubules.

1.4 Material and Methods

1.4.1 Yeast strains, culturing, and harvesting

Yeast strains used in this study can be found in the above Key Resources Table. Fluorescent tagging, degradation tags, and deletions were integrated as previously described (Longtine *et al.*, 1998; Lee, Lim and Thorn, 2013; Bindels *et al.*, 2017). All strains were grown in standard rich medium (YPD) at 25ºC since they contained a temperature-sensitive allele.

Cells were harvested as previously described in (Bergman *et al.*, 2018). In brief, strains were grown overnight in starter cultures and then diluted back into two identical 2L cultures of YPD at an OD600=6.25x10^{-3}. At an OD600=0.4 cultures were then shifted to 37ºC for a 3 hour arrest. Strains with degradation tags were treated with 250 μM 3-indole acetic acid (Sigma-Alrich, St. Louis, MO) in DMSO and 50 mM potassium phosphate buffer, pH 6.2, for 30 minutes before harvesting, 2.5 hours after the temperature shift. Cells were then harvested by serial centrifugation at 6000 x g in a Sorvall RC5B centrifuge using an SLA-3000 rotor for 10 minutes at 4ºC Cell pellets were then resuspended in cold ddH2O and pelleted in a Hermle Z446K centrifuge for 3 mins at 3430 x g at 4ºC This wash procedure was repeated once more, with any remaining liquid removed from the pellet via aspiration. Using a stainless steel lab spatula (Thermo Fisher, Waltham MA), the cells were then scraped out as small clumps into a 50 mL conical filled with liquid nitrogen, snap-freezing them, for storage at -80ºC.

1.4.2 Generation of whole cell lysates

As described previously by (Bergman *et al.*, 2018), approximately 5g of frozen cells were weighed into a pre-chilled medium-sized SPEX 6870 freezer mill vial (Spex, Metuchen, NJ). The pre-chilled chamber was then milled (submerged in liquid nitrogen) following a protocol that consisted of a 3 minute pre-chill, then 10 cycles of 3 minutes grinding at 30 impacts per second (15 cps) and 1 minute of rest. The resulting powered lysate was stored at -80ºC.

1.4.3 Generating stabilized far-red labeled tubulin seeds

As previously described in (Bergman *et al.*, 2018), purified bovine tubulin was cycled to remove nonfunctional tubulin. This tubulin was then mixed with both biotin-conjugated and HiLyte 647 labeled porcine tubulin (Cytoskeleton Inc., Denver, CO). The tubulin mix was then resuspended in PEM buffer (80 mM PIPES pH 6.9, 1 mM EGTA, 1 mM MgCl2) to a final concentration of 1.67 mg/mL unlabeled tubulin, 0.33 mg/mL biotin-labeled tubulin, and 0.33 mg/mL far-red labeled tubulin. To stabilize the seeds, GMPCPP (Jena Biosciences, Jena, Germany) was added to a final concentration of 1 mM. Aliquots were then snap-frozen in liquid nitrogen and stored at -80ºC.

1.4.4 Preparation of glass sides and passivation of coverslips

Both glass side preparation and passivation of coverslips followed the protocol previously described in (Bergman *et al.*, 2018). To prepare the glass sides for assembly into a flow chamber, microscope slides (Corning Inc., Corning, NY) were washed in acetone for 15 minutes and then 100% ethanol for 15 minutes. These slides were left to air dry before storage in an airtight container.

To prepare the coverslips for assembly into a flow chamber, cover glass (1.5 thickness, Corning Inc.) was first cleaned by sonication in acetone for 30 minutes. The coverslips were then soaked for 15 minutes in 100% ethanol. After 3 thorough, but short, rinses in ddH2O, the coverslips were submerged for 2 hours in 2% Hellmanex III solution (Hellma Analytics, Müllheim, Germany). After this, they were again rinsed in ddH2O three times. Before proceeding to passivation, the coverslips were blown dry with nitrogen gas. For passivation, a solution containing a 0.1 mg/mL mixture of PLL(20)-g[3.5]-PEG(2):PEG(3.4)-biotin(50%) (SuSoS AG, Dübendorf, Switzerland), at a ratio of 1:19, in 10 mM HEPES was prepared. 50 uL drops were then placed on Parafilm in a humid chamber and coverslips were gently placed onto the drops. After 1 hour, the passivated coverslips were washed for 2 minutes in PBS and rinsed in ddH2O for 1 minute. The coverslips were then air-dried with nitrogen gas and stored in an airtight container at 4ºC. These passivated coverslips were stored for use only for three weeks.

1.4.5 Assembly of flow chamber

Preparation and assembly of the flow chamber for use in the TIRF based dynamics assay was exactly as described in (Bergman *et al.*, 2018).

1.4.6 Preparation of whole cell lysates for dynamics assay

Similarly to what is described in (Bergman *et al.*, 2018), 0.22 g of powdered lysate was weighed out into a 1.5 mL Eppendorf tube pre-chilled in liquid nitrogen. To assemble microtubules of a physiologically desired length (~5 μm), a range of 1-25 μL of cold 10X PEM (800 mM PIPES pH 6.9,10 mM MgCl2, 10 mM EGTA) was added to the powered lysate, as some strains required more or less buffer volumes to obtain ~5 μm long microtubules in the assay. In addition to cold 10X PEM, 0.5 μL of Protease Inhibitor Cocktail IV (Calbiochem, San Diego, CA) and 4 μL of 25.5 U/μL benzonase nuclease (EMD Millipore, San Diego, CA, prod. 70746-3, >90% purity) was added, spun down

briefly, and thawed on ice for 10 minutes. Lysate was added to pre-chilled polycarbonate ultracentrifuge tubes and cleared of insoluble material by spinning at 34,600 x g for 25 minutes at 4ºC. After ultracentrifugation, 32 µL of cleared lysate supernatant was flowed into the chamber prepared previously (see above).

1.4.7 TIRF Microscopy

After clarified lysate supernatant was added to the prepared chamber, the slides were loaded onto a Nikon Ti2-E inverted microscope with an Oko Labs environmental chamber pre-warmed to 28ºC. Images were acquired using a Nikon 60X CFI Apo TIRF objective (NA 1.49) and an Orca Fusion Gen III sCMOS camera (Hamamatsu, Hamamatsu City, Japan) at 1.5X magnification using the Nikon NIS Elements software. Using a LUNF 4-line laser launch (Nikon Instruments, Melville, NY) and an iLas2 TIRF/FRAP module (Gataca Systems, Massy, France) total internal reflection fluorescence (TIRF) illuminated a single focal plane of the field and was imaged every 5 seconds for 30 minutes.

1.4.8 Sequential lysate flow assays

Similar coverslip, slide, assembly of flow chamber, and lysate preparation were all followed as described above. However, instead of preparing one lysate for one genotype, two lysates were prepared side-by-side. To observe the initial behavior, 32 µL of the first lysate was flowed through the chamber and imaged for 10 minutes. While the slide was still mounted on the microscope, the movie was paused for 1 minute while the second lysate was carefully flowed in, replacing the first. After replacing the lysate, the movie was restarted and the same field of view was captured for another 20 minutes.

1.4.9 *In vivo* live cell microscopy

Cells were grown in rich medium (YPD) overnight to saturation at 25ºC. The next day the cells were diluted into fresh YPD and grown for ~4 hrs (2 doublings) at 25ºC, until the culture reached log phase (OD600=0.5). They were then spun down and washed with minimal Imaging Medium three times (synthetic minimal medium supplemented with 20 µg/ml adenine, uracil, L-histadine and L-methionine; 30 µg/ml L-leucine and L-lysine; and 2% glucose; Sigma-Aldrich). Cells were then immobilized on coverslips coated with 0.2 mg/ml concanavalin A and were imaged in Imaging Medium. Using a Nikon Ti2-E inverted microscope with an Oko Labs environmental chamber pre-warmed to 25ºC. Images were acquired with a Nikon 60X CFI Apo TIRF objective (NA 1.49) and an Orca Fusion Gen III sCMOS camera (Hamamatsu) at 1.5X magnification using the Nikon NIS Elements software. For imaging, a LUNF 4-line laser launch (Nikon) and an iLas2 TIRF/FRAP module (Gataca Systems) was used for HiLo total internal reflection fluorescence (Tokunaga2008). Images were taken with 0.2 µm slices for a total 5 µm Z-stack.

1.4.10 Image and data analysis

For the microtubule dynamics assay, analysis was done as described previously in (Bergman *et al.*, 2018). Imaging data were analyzed using Fiji software (NIH). Registration

to correct for stage drift was applied to the raw data (StackReg; (Thévenaz, Ruttimann and Unser, 1998). Kymographs were generated from all microtubules for which the entire length could be tracked for the entire movie. Kymographs were excluded if the microtubules were crossed or bundled. For analysis, data from independent technical trials and biological replicas from one genotype were pooled, unless otherwise indicated. In our quantification of speeds, a minimum threshold of 86.7 nm/min for kinetochore movement rates was established based on the resolution of the kymographs used to measure speed. Kinetochore movements less than a threshold slope of 1pixel displacement (72.2 nm) per 10 pixels of time (50 sec) were categorized as “paused”. Velocities are reported as mean with the standard error of the mean. Statistical significance was determined using a Kruskal-Wallis test (GraphPad Prism, San Diego, CA). P Values are reported as in the figure captions.

For the colocalization quantification, pair-wise kinetochore tracks (that moved as defined above) were pooled into three categories (always, partially, and never colocalized) based on the amount of time that the two proteins were colocalized. Because the red fluorophore blinked, colocalization was scored solely for the mScarlet tagged protein (either Ndc80 or Mtw1).

For the live cell imaging analysis, images were analyzed using Fiji (NIH). Maximum intensity Z-projections were made and bleach corrections were applied using the “histogram matching” macro. Metaphase cells were identified by the presence of a 2-3 μm spindle at the entrance to the bud neck. Cells were then counted as either “bilobed” or “declustered” based on the presence of two distinct kinetochore puncta. Line scans were done to assist in this binary classification. If two clear peaks were present, the cell was “bilobed.” Any other line scan shape, i.e., 3+ peaks or 1 long kinetochore signal that matched the spindle, were classified as “declustered.” Data are from two independent technical trials of one biological replicate. In each replicate, n = 50 cells were counted. Graphs are of the mean and standard error of the mean (GraphPad Prism).

1.4.11 Cryo-sample preparation

Holey carbon electron microscopy grids (Quantifoil R2/1, 200 mesh, copper; Electron Microscopy Science, Hatfield, PA) were washed in 99.5% acetone while agitating on a rocker for 15 to 30 min to remove potential residual plastic backing, then washed in H2O, and dried with filter paper. Cell lysate of DDY5818 (*cdc23-1*, SPC105-3xFlexLinker-yoEGFP, mRuby2-TUB1) strain was prepared as described above. After ultracentrifugation, supernatants were aliquoted into pre-chilled microcentrifuge tubes with a volume of 9.5 μL supernatant per aliquot and kept on ice. About 15 minutes before the lysate centrifugation was finished, far-red labeled GpCpp-stabilized MT seeds were polymerized in microcentrifuge tubes at 37°C for 10 min. Grids were coated with 10 nm BSA Gold Tracer (Electron Microscopy Sciences) by dripping a total of 10 to 20 μL of the BSA Gold Tracer solution on the grids and removing the drops with filter paper. Seeds were diluted 1/50 in 1X PEM buffer. 0.5 μL of seeds were mixed with 9.5 μL cleared lysate. 3-6 μL of the mix were pipetted on the pre-coated grids. For sample vitrification, either a Vitrobot Mark IV (FEI, Hillsboro, OR) or a Leica EM GP2 (Leica Microsystems, Wetzlar, Germany) was used. Sample chamber conditions were set to

28ºC and 75-90% humidity. Samples were incubated in the sample chamber for 10-15 min and then blotted from the backside and vitrified by plunging into liquid ethane. To set up the Vitrobot Mark IV for back-blotting, the filter paper facing the sample side was replaced with a custom-made Teflon sheet of the same size to blot only the fluid from the back of the sample. To ensure that suitable grids were produced for each imaging session, a range of plot forces between 0 and 10 (for Vitrobot Mark IV only), blotting times of 3 to 6 s, and a 1 s drain time, were used. Grids were fixed into AutoGrid carriers (Thermo Fisher) and stored in liquid nitrogen until they were imaged.

1.4.12 Cryo-fluorescence light microscopy

Cryo-samples were imaged on a Leica EM Cryo CLEM system (Leica Microsystems). The system consists of a Leica DM6 FS widefield microscope that is equipped with a motorized Leica EM Cryo stage and a short working distance (<0.28 mm) 50x Leica EM Cryo CLEM ceramic tipped objective (numerical aperture = 0.90). These specifications allow sample imaging at liquid nitrogen temperatures. A halogen lamp powered by a CTR6 halogen supply unit was used as a light source. We used GFP ET (Excitation: 470/40, Dichroic: 495, Emission 525/50), RFP (Excitation: 546/10, Dichroic: 560, Emission 585/40) and Y5 (Excitation: 620/60, Dichroic: 660, Emission 700/75) filter cubes for imaging. For cryo-correlative light and electron microscopy, a grid overview map was recorded using transmitted light and Y5 or GFP channels. The map was used to identify grid squares with good ice quality and intact carbon film. Z-stacks (total Z = ~7 µm in 0.5 µm steps) of regions with clear fluorescence signals were recorded using the transmitted light, GFP (Spc105), RFP (Tub1) and Y5 (seeds) channels. These images were used to identify Spc105-GFP positive regions of interest for subsequent cryo-electron tomography imaging. The same imaging conditions were used for grid squares on individual grids. Imaging conditions were varied between grids to obtain sufficient signal to allow correlation in later steps. Images for panel generation in Adobe Illustrator were prepared using Fiji and Adobe Photoshop. No nonlinear gamma correction was applied during image processing.

1.4.13 Cryo-electron tomography data acquisition and tomogram reconstruction

Samples were imaged on a Titan Krios transmission electron microscope (FEI) equipped with an X-FEG electron source, a BioQuantum energy filter (Gatan, Pleasanton, CA) and a K3 direct electron detecting device (Gatan) and operated at 300 kV. Samples were visually inspected for ice quality using the FEI flu cam. Overview grid maps were acquired at ~0.2 µm pixel size. These grid maps were used to identify grid squares of interest from the cryo-fluorescence light microscopy overview maps. Grid square images and polygon maps of the regions of interest with an overlap of 20-25% between individual images were recorded. The polygon maps were used to pick tilt series acquisition points based on the fluorescent signal from cryo-fluorescence light microscopy. The hole pattern of the carbon film was used as a guide. Acquisition points were chosen with adequate distance between individual points to prevent electron dose exposure damage prior to data collection. SerialEM (Mastronarde, 2005) in low-dose mode was used for automatic tilt-series recording using a bidirectional tilt scheme starting at +20º and with a typical

tilt range from +60º to -60º and base increment of 2º. Pixel sizes between 2.63 and 3.07Å were used. Target defocus was varied between -2 and -x µm and the targeted total electron dose was 100 e-/Å^2. Data were collected in 0.5 binning mode or without binning. Frame time was 0.2 – 0.25 s. Tilt series alignment and tomogram reconstruction were done using the freely available IMOD software package (Kremer1996). Tilt series were aligned using 10 nm gold particles as fiducials and tomograms were reconstructed using the backprojection algorithm combined with the SIRT-like filter. Tomograms were then filtered using the Nonlinear Anisotropic Diffusion filter and binned by a factor of 3 or 4 using the binvol function in IMOD to further increase contrast for analysis and visualization. Images for panel generation in Adobe Illustrator were prepared using IMOD and Adobe Photoshop. No nonlinear gamma correction was applied during image processing.

Chapter Two

Interdependence of a microtubule polymerase and a motor protein in establishment of kinetochore end-on attachments

2.1 Introduction

Mitosis is an essential process by which replicated chromosomes are segregated to daughter cells. To achieve this, chromosomes are physically partitioned into daughter cells via a microtubule-mediated process. Through a complex process involving microtubule assembly and disassembly, combined with actions of kinesin and dynein motor proteins, forces first align the chromosomes on the metaphase plate and then separate the sister chromosomes to the two spindle poles. Spindle microtubules attach to a specialized protein structure assembled on centromere DNA called the kinetochore. The kinetochore binds both to the sides and plus ends of microtubules and can move along microtubules via lateral interactions with the microtubule lattice. It also can move in association with the microtubule plus end and allows tubulin association and dissociation with the plus end while remaining tightly bound (Biggins *et al.*, 2013).

The process by which chromosomes align at the center of the mitotic spindle for proper partitioning is called chromosome congression (Maiato *et al.*, 2017). Chromosome congression is a very complex process dependent upon motor forces (Cottingham *et al.*, 1999), spindle geometry (Risteski *et al.*, 2021), post-translational modifications (Barisic and Maiato, 2016), and chemical gradients (Heald and Khodjakov, 2015). Many studies have addressed the roles of motor proteins in chromosome congression, especially in mammalian cells. Dynein, a minus-end directed microtubule motor protein, pulls chromosomes along astral microtubules toward the centrosome, facilitating attachment of kinetochores to microtubule plus ends (Kapoor *et al.*, 2006; Li *et al.*, 2007). Chromosomes that do not make end-on, plus end, attachment to kinetochore-microtubules can be transported to the plus-end by a kinesin-7, CENP-E (Lemura and Tanaka, 2015; Craske and Welburn, 2020). When CENP-E is chemically inhibited in cells, kinetochores do not align on the metaphase plate. Instead, many chromosomes remain near the poles, with their distribution spanning the entire spindle length, resulting in mitotic arrest and even cell death (Barisic *et al.*, 2015).

In budding yeast, several proteins have been shown to provide functions similar to those implicated in facilitating chromosome congression in mammals. The yeast minus end-directed kinesin-14, Kar3, is functionally analogous to dynein, moving chromosomes toward the spindle pole body (Tanaka *et al.*, 2005). Our previous research provides evidence that the yeast kinesin-8, Kip3, has a function similar to CENP-E. When Kip3 is absent in cells, kinetochores are spread along the mitotic spindle rather than aligned along the metaphase plate (Torvi *et al.*, 2022). Additionally, Kip3 absence from in vitro assays results in loss of plus end-directed kinetochore motility (Torvi *et al.*, 2022). However, the molecular mechanism by which Kip3 mediates kinetochore motility remains a mystery. Kinetochores move along microtubules much more slowly than Kip3

itself. Additionally, kinetochores frequently pause on the microtubule lattice, whereas Kip3 movement is constant. Therefore, Kip3-mediated kinetochore transport along microtubules appears distinct from behavior observed for transport of other cargos along microtubules by motor proteins. Here we set out to further explore Kip3's involvement in kinetochore motility.

One candidate for a protein that might mediate Kip3's role in kinetochore motility is the microtubule polymerase, Stu2. Split fluorescent protein assays, yeast two-hybrid screens, and immune-purifications indicate that Kip3 and Stu2 interact physically (Gandhi *et al.*, 2011). In addition to Stu2's microtubule polymerase function, Stu2 has recently been shown to have a role at the kinetochore facilitating proper microtubule attachments. Through immune-purifications, binding assays, cross-linking mass spectrometry, and crystallography, Stu2 has been shown to bind to kinetochores via interaction with the Ndc80 complex and aide in the establishment of proper kinetochore-microtubule attachments (Miller, Asbury and Biggins, 2016; Miller *et al.*, 2019; Zahm *et al.*, 2021). However, we recently showed that, unexpectedly, Stu2's essential function is not its microtubule polymerase activity, but rather an as-yet-to-be defined function that requires nuclear localization (Carrier *et al.*, 2022). Given that Kip3 binds to Stu2, and that Stu2 can bind to the kinetochore, we set out to explore possible functional interdependence between Kip3 and Stu2 in kinetochore motility during congression. Using the assay we developed previously to observe single kinetochores moving on microtubules, and to implicate Kip3 in this process, we now investigated possible Kip3-Stu2 functional cooperation during kinetochore motility (Bergman *et al.*, 2018; Torvi *et al.*, 2022).

2.2 Results and discussion

2.2.1 Stu2 is required for kinetochore movement toward the microtubule plus end

Previously we reported that kinetochores bind to microtubules in metaphase-arrested cell lysates and translocate on the lateral surface toward the plus end (Torvi *et al.*, 2022). While kinesin-8, Kip3, absence from lysates resulted in immobile kinetochores, the mechanism of lateral directional kinetochore motility was, nevertheless, not clear since the kinetochore movement rate was markedly slower than Kip3's velocity. Here, we further investigated this mechanism by determining if Stu2, a protein that binds both to kinetochores and to Kip3, is involved in this process. Briefly, using our reconstitution assay (Bergman *et al.*, 2018; Torvi *et al.*, 2022), which uses cell-cycle arrested whole cell lysates, we observed dynamic kinetochores and MAPs on microtubules via TIRF microscopy. Kinetochore proteins (Spc105) and MAPs (Kip3, Stu2) were expressed at endogenous levels as fusions to fluorescent proteins in a strain background with fluorescently tagged alpha-tubulin (Tub1) and a temperature sensitive mutant (cdc23-1) that causes cells to arrest in metaphase at the non-permissive temperature (Irniger *et al.*, 1995).

As we reported previously, in wild-type lysates, kinetochores (tracked by imaging Spc105-GFP), bind to the lateral surface of microtubules and move in a processive, directional manner toward the microtubule plus end at a speed of 0.57±0.041 μm/min

and average run length of 0.81±0.059 μm (Torvi *et al.*, 2022) (Figure 2.1a-d). When bound to the lattice, the kinetochores spend most of the time stationary, but spend ~36% of the time moving toward the plus-end, and <1% of the time moving toward the minus-end (Figure 2.1b). Due to both kinetochore movement toward the plus end and microtubule plus end dynamic assembly and disassembly (Bergman *et al.*, 2018), kinetochores eventually reach microtubule plus-ends and establish end-on attachments. Once a kinetochore is bound to the microtubule plus end, that end is never observed to resume growth. Instead, kinetochore-bound plus ends are either paused (~81% of the time) or shrinking (~19%) (Torvi *et al.*, 2022) (Figure 2.1 a and b).

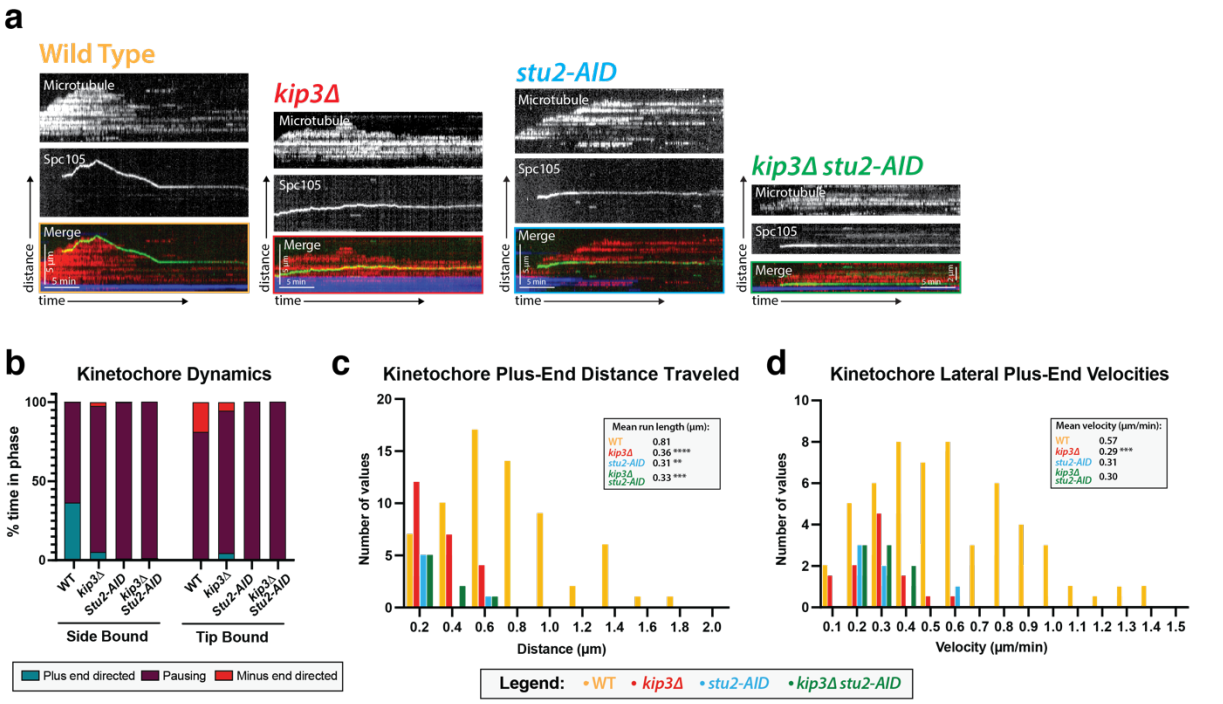

Figure 2.1 Kip3 and Stu2 are required for lateral kinetochore movement on metaphase microtubules (a) Kinetochore movement toward the microtubule plus end is dependent on Kip3 and Stu2. Representative kymographs from metaphase-arrested lysates with Spc105-GFP, an outer kinetochore protein. Time is on the x-axis and distance is on the y-axis (scale bars are 5 min and 5 μm, respectively). The kinetochore (Spc105-GFP) is shown in green, the yeast microtubule (mRuby2-Tub1) is red, and the stabilized microtubule seed is blue. In wild-type lysates kinetochores toward the microtubule plus-end when bound to the microtubule lateral surface and track the microtubule tip after becoming end-bound. (b) Quantification of dynamics over time shows that kinetochores spend 36.16% of their time moving toward the plus-end of the microtubule when laterally bound to the microtubule. This value decreases to 5.18%, 1.13%, and 1% in *kip3Δ, stu2-AID,* and *kip3Δ stu2-AID* lysate, respectively. Additionally, when a kinetochore reaches the microtubule end in a mutant lysate, reduced tip-bound, minus-end directed kinetochore movement is observed compared to wild-type lysate. (c) Both run lengths and the number of runs the kinetochores make toward the microtubule plus-ends depend on Kip3 and Stu2. While the wild-type run length was 0.81 μm in *kip3Δ, stu2-AID,* and *kip3Δ stu2-AID* lysate lysates showed run lengths reduced to 0.36 μm, 0.31 μm, and 0.33 μm, respectively. Statistical analysis was done by a Kruskal-Wallis test, wherein **** is p <0.0001, *** is p = 0.0005, and ** is p = 0.0021. (d) Laterally bound kinetochore velocities were reduced from 0.57 μm/min to 0.29 μm/min, 0.31 μm/min, and 0.30 μm/min in *kip3Δ, stu2-AID* and *kip3Δ & stu2-AID* lysates, respectively. Statistical analysis was done using a Kruskal-Wallis test where *** is p=0.0004. (b-d) Quantification is from two replicate trails. For each strain from WT to *kip3Δ & stu2-AID* lysate in the order listed, N=42, 47, 38, and 46 Spc105-GFP proteins tracked.

So far, based on our previous observations of mutants of all yeast kinesins, we found that only the kinesin-8 Kip3 (Torvi *et al.*, 2022) is necessary for motility. Here, we found that the microtubule polymerase, Stu2 (Figure 2.1), is also necessary for the directional and processive movement toward the plus end of the kinetochore bound to the microtubule lattice. When Kip3, Stu2, or both of these proteins, is absent, motility is defective (Figure 2.1a). In the three mutant lysates: *kip3Δ, stu2-AID,* and *kip3Δ stu2-AID* mutant, the kinetochore run lengths decreased to 0.36±0.28, 0.31±0.040, and 0.33±0.045 μm, respectively (Figure 2.1c). Similarly, the kinetochore velocities decreased to 0.29±0.028, 0.31±0.051, and 0.30±0.031 μm/min, respectively (Figure 2.1d). Lastly, we observed altered microtubule dynamics when Kip3 and Stu2 were removed. Both proteins have known microtubule dynamics functions, which have been characterized previously (Su *et al.*, 2011; Ayaz *et al.*, 2012; Arellano-Santoyo *et al.*, 2017) and also analyzed using this assay (Bergman *et al.*, 2018; Carrier *et al.*, 2022). Kip3 is a catastrophe factor, so microtubules depolymerize less in the *kip3Δ* (Bergman *et al.*, 2018). Stu2 is microtubule polymerase and also contributes to microtubule catastrophe, so we also observe microtubules in a *stu2-AID* growing slowly and rarely depolymerizing (Carrier *et al.*, 2022). Interestingly, the loss of Kip3 and Stu2, individually or together, also abolishes tip-bound kinetochores moving with shrinking microtubules, implying that these MAPs are necessary for *both* lateral kinetochore movement and kinetochore-induced microtubule depolymerization (Figure 2.1b).

2.2.2 Distinct Kip3 and Stu2 dynamics on microtubules in metaphase lysates

Given that the absence of either Kip3 or Stu2 alone, or in combination, results in kinetochores that no longer move processively on the microtubule lattice, we next characterized the dynamics of these proteins in metaphase-arrested lysates to look for evidence of a functional relationship. As shown previously (Bergman *et al.*, 2018; Torvi *et al.*, 2022), Kip3 is highly abundant on microtubules and walks processively toward the microtubule plus-end at a velocity of 2.8±0.047 μm/min without pausing (Figure 2.2a). Additionally, the fluorescence intensity of Kip3 on the growing microtubule end was about twice as high as on the shrinking microtubule end (Figure 2.2a). This dynamic behavior in metaphase arrested lysates is distinct from the behavior observed in lysates of cells arrested in other cell cycle stages (Figure 2.3a). In S-phase and anaphase lysates, Kip3 was not processive and came on and off the microtubule dynamically. In conclusion, Kip3 processivity and plus-end accumulation were specific to metaphase-arrested lysates.

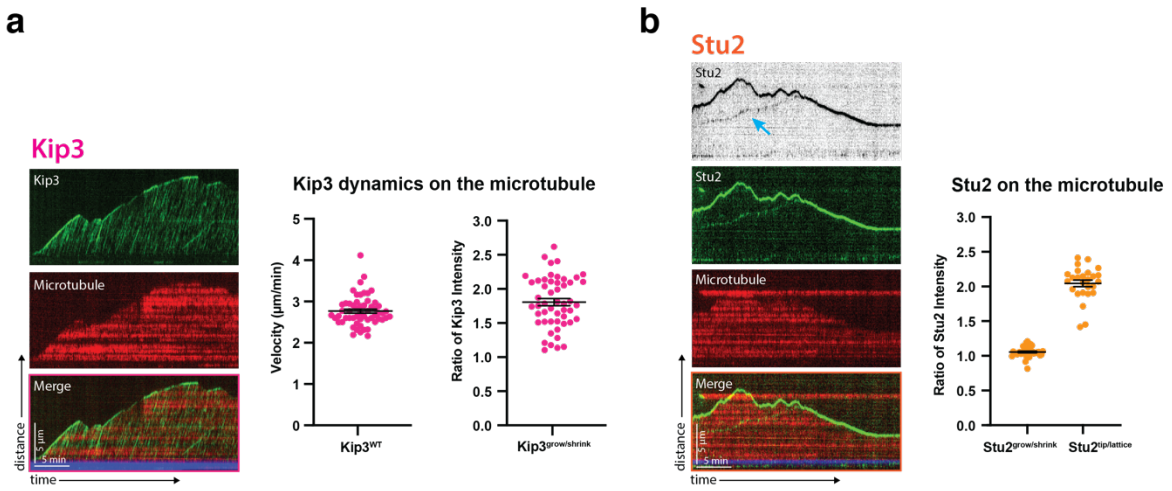

Figure 2.2 Distinct Kip3 and Stu2 dynamics on the metaphase microtubule (a) Representative kymograph showing Kip3-GFP in green, the yeast microtubule (mRub2-Tub1) in red, and the porcine seed in blue in a metaphase-arrested lysate. Time is on the x-axis and distance is on the y-axis (scale bars are 5 min and 5 μm, respectively). Processive Kip3 tracks are seen streaming along the microtubule with Kip3 accumulation at the plus ends of growing microtubules. The mean velocity of Kip3 is 2.8 μm/min and the ratio of Kip3 fluorescent intensity on growing microtubule ends compared to shrinking ends is 1.8. On both graphs the SEM is indicated in black. (b) Representative kymograph showing Stu2-GFP in green, the yeast microtubule (mRuby2-Tub1) in red, and the porcine seed in blue in a metaphase-arrested lysate. Time is on the x-axis and distance is on the y-axis (scale bars are 5 min and 5 μm, respectively). Stu2 tracks both the growing and shrinking ends of microtubules. Additionally, a dimmer Stu2 signal is apparent on the microtubule lattice, slowly moving toward the tip in a unidirectional manner (blue arrow). This localization is quantified in the graph to the right, where the ratio of Stu2 fluorescence intensity at growing and shrinking microtubule ends is 1.05 and the ratio at the tip compared to the lattice is 2.05. The SEM is indicated in black.

The dynamics of Stu2 were distinct from those of Kip3. As previously reported, we observed Stu2 associated with the microtubule tip where it acts as a polymerase, binding tubulin dimers and facilitating their addition to the growing end (Geyer *et al.*, 2018). Interestingly, we also observed that the amount of Stu2 on the tip of polymerizing versus depolymerizing microtubules was equal and steady over time (Figure 2.2b), a novel characterization not yet observed. This characteristic is notably different from other plus-tip associated proteins like Bim1/EB1 in *in vitro* assays (Vaughan *et al.,* 2005) since those proteins predominantly associate with growing microtubule ends. In addition to observing Stu2 on microtubule plus ends, we observed a fainter Stu2 signal moving slowly along the microtubule lattice towards the plus-end. Compared to the fluorescent intensity of Stu2 at the microtubule tip, the lattice-bound Stu2 signal was about half as bright (Figure 2.2b). Another difference when compared to Kip3 was that Stu2 dynamics were unchanged throughout the cell cycle. In all cell cycle stages tested, Stu2 remained on both growing and shrinking microtubule ends, and there was frequently a dimmer lattice-bound signal (Figure 2.3b). However, processive plus-end-directed movement of Stu2 along microtubules was only observed in metaphase-arrested lysates. For this reason, we focused the rest of our investigation of the roles of Kip3 and Stu2 in metaphase.

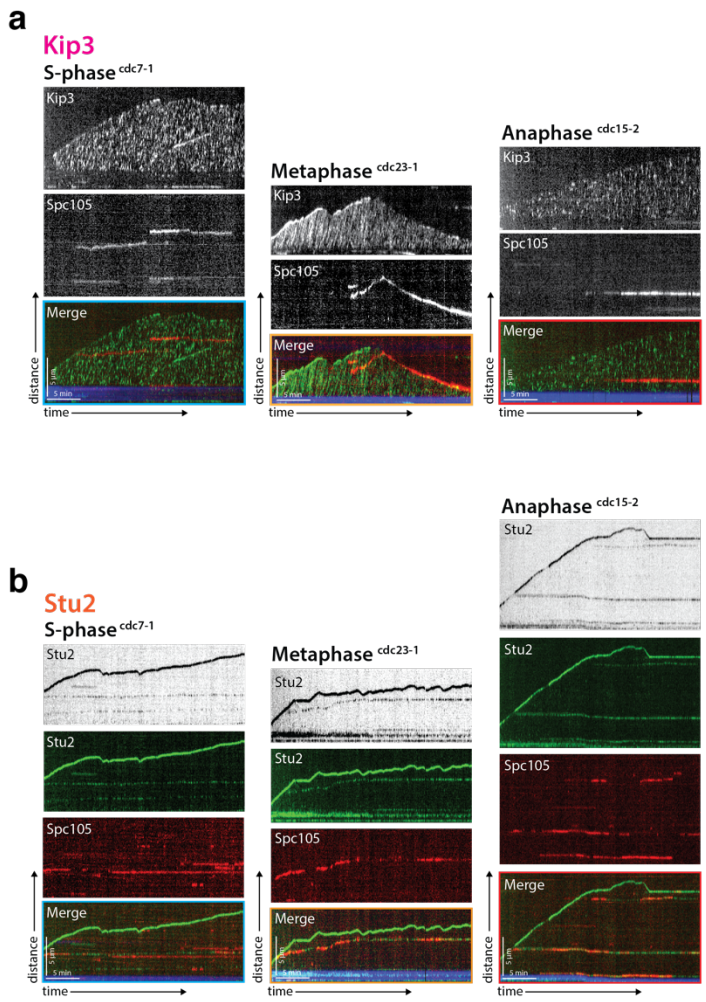

Figure 2.3 Kip3, Stu2, and the kinetochore dynamics in different cell cycle stages (a) Representative kymographs with Kip3-GFP in green, Spc105-mScarlet in red, and the porcine seed in blue. Time is on the x-axis and distance is on the y-axis (scale bars are 5 min and 5 μm, respectively). Kip3 either comes on and off the microtubule dynamically (S-phase and anaphase) or streams along the microtubule processively (metaphase). (b) Representative kymographs with Stu2-GFP in green, Spc105-mScarlet in red, and the porcine seed in blue. Time is on the x-axis and distance is on the y-axis (scale bars are 5 min and 5 μm, respectively). Stu2 tracks both the growing and shrinking microtubule tip irrespective of the cell cycle stage. When Stu2 is detected on the lattice, it is invariably colocalized with the kinetochore, marked by Spc105-mScarlet. (a and b) Each panel represents different cell cycle arrests using temperature sensitive *cdc* alleles; *cdc7-1* for S-phase, *cdc23-1* for metaphase and *cdc15-2* for anaphase. In metaphase arrested lysates kinetochores, marked by Spc105-mScarlet, are only observed to move toward plus ends, or to track plus ends (Torvi Wong 2022).

2.2.3 Stu2 co-localizes with kinetochores in vitro and acts with Kip3 to facilitate lateral kinetochore movement

We hypothesized that Kip3, Stu2, and kinetochores might associate to facilitate kinetochore motility. To test this possibility, we imaged Kip3-GFP and Stu2-GFP in combination with a fluorescently tagged kinetochore protein, Spc105-mScarlet, and looked for co-localization in lysates made from cells arrested at metaphase. Based on the dynamics of the faint Stu2 signal we observed on lateral microtubule surfaces (Figure

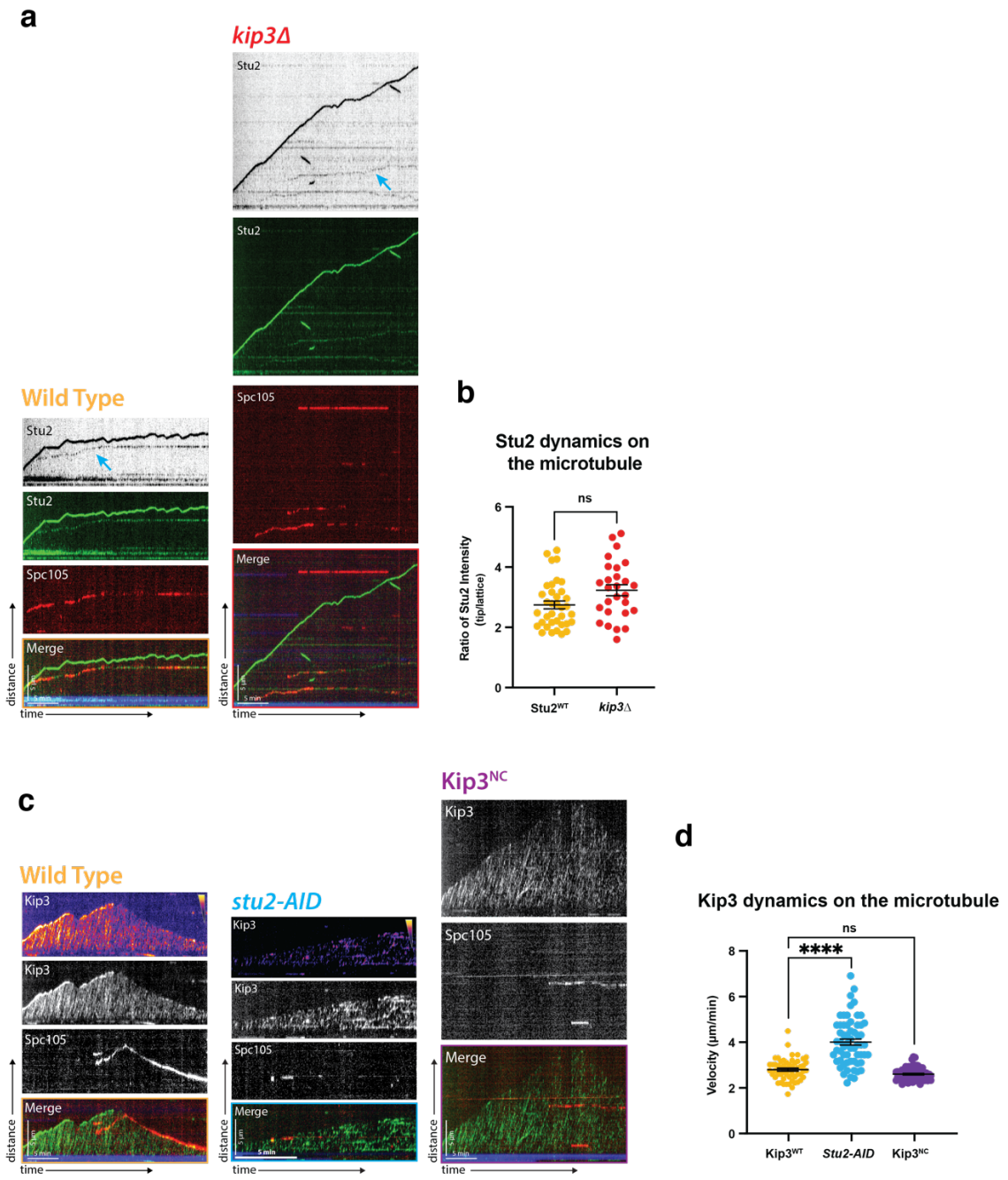

Figure 2.4 Kinetochore movement toward microtubule plus end depends on Kip3 and association with Stu2 (a) Representative kymograph showing metaphase arrested lysate with Stu2-GFP in green, Spc105-mScarlet in red, and the porcine seed in blue. Time is on the x-axis and distance is on the y-axis (scale bars are 5 min and 5 μm, respectively). In wild-type lysate one population of Stu2 tracks the microtubule tip and the other colocalizes with kinetochores. In a *kip3Δ* lysate, stu2's association with kinetochores is independent of Kip3. (b) Fluorescence intensity of Stu2 at the microtubule tip is 2.8 fold greater than Stu2 associated with kinetochores on the microtubule lattice in wild-type lysates. This ratio is essentially unchanged when Kip3 is absent, with only a statistically insignificant increase to 3.2. The SEM is shown in black. Statistical analysis was done using a Kruskal-Wallis test where ns is p=0.1145. Quantification is from two replicate trials. For lysates from each strain, WT and *stu2-AID,* N=36 and 27, number of Stu2-GFP signals quantified. (c) Representative kymograph from lysate made from metaphase-arrested cells with Kip3-GFP in green, Spc105-mScarlet in red, and the porcine seed in blue. Time is on the x-axis and distance is on

the y-axis (scale bars are 5 min and 5 μm, respectively). In wild-type lysate, Kip3 moves faster than the kinetochore on the microtubule lattice with no detectable colocalization. When Stu2 is depleted, the kinetochore does not move, but Kip3 moves faster with shorter run lengths. When the Kip3 neck chimera variant replaces the wild-type protein, microtubule-associated kinetochores do not move, but Kip3 is still processive, though it no longer accumulates on growing microtubule ends. (d) Kip3 velocities were quantified revealing that Kip3 moves faster upon Stu2 depletion, showing an increase in velocity from 2.8 μm/min to 4.0 μm/min. Additionally, $Kip3^{NC}$ did not show altered speed relative to the wild-type protein, with a velocity of 2.6 μm/min. The SEM is shown in black. Statistical analysis was done using a Kruskal-Wallis test where **** is $p<0.0001$. Quantification is from two replicate trials. For each strain in the order listed from WT to $Kip3^{NC}$ lysate, N=57, 61, and 64 Kip3 proteins were tracked.

2.2b), we hypothesized that this signal might represent a kinetochore-bound pool. When visualizing Stu2-GFP in combination with Spc105-mScarlet, we observed that, invariably, the faint lattice-bound Stu2 colocalized with the Spc105 (Figure 2.4a). In sharp contrast, as reported previously (Torvi *et al.*, 2022), Kip3 moves much faster than the kinetochore and no Kip3 signal was ever detected moving along with the kinetochore, although there is frequent overlap of the kinesin's tracks with those of Spc105 (Figure 2.4c).

Although no colocalization between Stu2 and Kip3 was detected, we wished to further test the possibility that Stu2 acts as a bridge between Kip3 and the kinetochore since these two proteins have been reported previously to interact with each other. To do this, we tested whether Stu2 localization at kinetochores was dependent on Kip3. When the gene encoding Kip3 is deleted, kinetochores do not move on the microtubule (Figure 2.1) and microtubules undergo much less frequent catastrophes (Bergman *et al.*, 2018). However, Stu2 colocalization with kinetochores was not detectably altered in this mutant. In the absence of Kip3, Stu2 is still associated with both the growing and shrinking microtubule ends and still colocalizes with kinetochores. Also, the ratio of the intensity of Stu2-GFP at microtubule ends to the intensity at the kinetochore was not detectably different between wild-type and *kip3Δ* lysates, although TIRF is an imperfect approach for making such ratio-metric determinations (Figure 2.4b).

Given that Stu2 is still at the kinetochore when Kip3 is absent (Figure 2.4b) and that kinetochores do not move when Stu2 is absent (Figure 2.1), we hypothesized that Stu2 connects Kip3 to the kinetochore. We predicted that, if we were to observe Kip3 and the kinetochore in the absence of Stu2, Kip3 would show wild-type dynamics. Surprisingly, this was not the case. When Stu2 is absent, as reported above, kinetochores become immobile (Figure 2.1), microtubule growth slows and depolymerization decreases (Carrier *et al.*, 2022). However, Kip3 dynamics were also severely altered (Figure 2.4c). Instead of non-stop runs at a velocity of 2.8±0.064 μm/min, runs become very short and increase in velocity to 4±0.13 μm/min in the absence of Stu2 (Figure 2.4d; note the 2x acquisition rate of the movies in Figure 2.4c required because of the faster Kip3 motility rates). Additionally, there was less Kip3 bound to microtubules when Stu2 was absent, as shown by the heatmap of Kip3 in kymographs (Figure 2.4c). Finally, there was a pronounced diminution of Kip3 accumulation at microtubule plus ends in this mutant. Additionally, we were able to show that the addition of wild-type Stu2 lysate back to a *stu2-AID* lysate restored Kip3 processivity (Figure 2.5a). Reversing this sequence, when *stu2-AID* lysate was replaced by a lysate with wild-type Stu2, Kip3 processivity was instantly diminished (Figure 2.5b). These results indicate that Stu2 absence affects more than just kinetochore motility along microtubules in this lysate

assay. While kinetochores are immobile in a Stu2-depleted lysate, this could be because either it mediates the interaction between Kip3 and the kinetochore or that it affects Kip3 motility, which then results in the loss of kinetochore motility (see Conclusion 2.3).

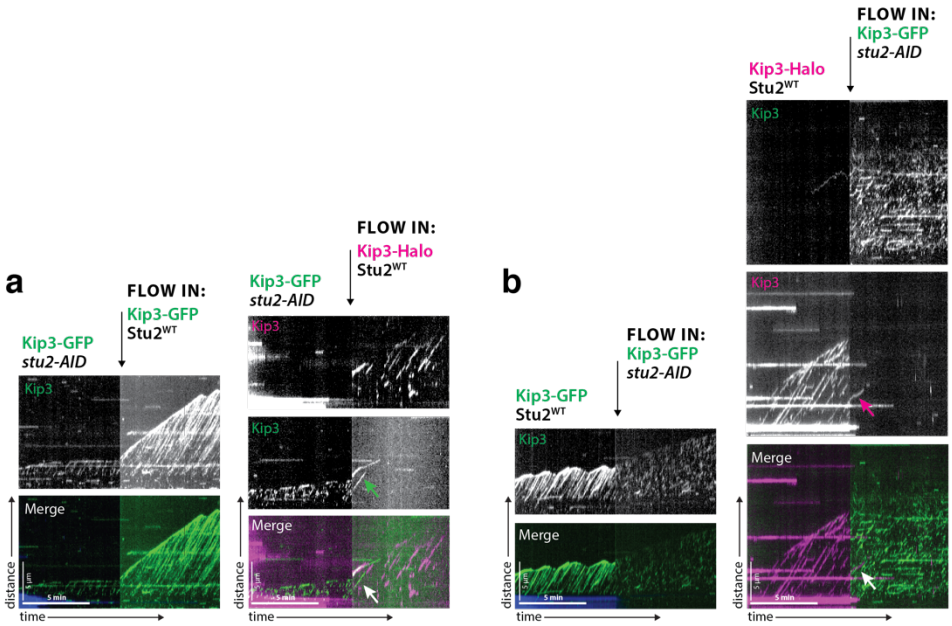

Figure 2.5 Flow through Stu2 add back to asses Kip3 motility (a) Kip3-GFP was imaged in a *stu2-AID* lysate showing short non-processive motor tracks. Lysate containing wild type Stu2 was added back to the imaging chambers and the Kip3 processivity was tracked either with a Kip3-GFP (left) or with a far red Kip3-Halo (right). Arrows show areas in which Kip3 from the *stu2-aid* strain restored processivity once wild-type Stu2 was added. (b) Kip3-GFP (left) or far red Kip3-Halo (right) was imaged in wild-type Stu2 lysate showing long processive motor tracks. Lysate from *stu2-AID* strains, depleted for Stu2, replaced the wild-type lysate in the imaging chambers and the Kip3 processivity was tracked with Kip3-GFP. Arrows show areas in which Kip3 from the wild-type Stu2 strain lost processivity once *stu2-AID* lysate was added in.

As another approach to exploring the functional relationship between Stu2 and Kip3, we next attempted to create a Kip3 separation-of-function mutant. Given that we previously found that kinetochores were still motile in a Kip3 mutant lacking the entire tail (amino acids 482-805) (Torvi *et al.*, 2022), we turned our attention to the 42 amino acid neck-linker (amino acids 439-481). Based on earlier reports that Kip3 amino acids 1-446 can bind to Stu2 (Gandhi *et al.*, 2011), we narrowed our target to amino acids 439-446. Kinesin neck linker sequences are very important for dictating the motor's processivity (Kim, Fonseca and Stumpff, 2014; Malaby *et al.*, 2019). We therefore did not want to mutate the neck in a way that would disrupt its structure. We substituted amino acids 439-446 with those from another similarly processive kinesin, Kif18a, a mammalian kinesin-8 that shares many similarities to Kip3, both in structure and function (Stumpff *et al.*, 2008, 2011). Therefore, we created a Kip3-Kif18a neck-chimera (Kip3^{NC}) replacing amino acids 439-446 in Kip3 with those of Kif18a (Figure 2.6a). Mutating these six amino acids in the neck of Kip3 resulted in a motor with wild-type processivity (Figure 2.4c and d), but resulted in immobile kinetochores (Figure 2.4c). Interestingly, this Kip3^{NC} protein no longer accumulated on the plus-ends of microtubules. These microtubules also

exhibited a lower catastrophe frequency, consistent with loss of a previously reported Kip3 activity (see Conclusion 2.3). Despite this unintended plus end-associated phenotype and our current inability to determine whether this mutant can bind to Stu2, we can conclude that these six amino acids in the neck-linker are necessary for kinetochore motility.

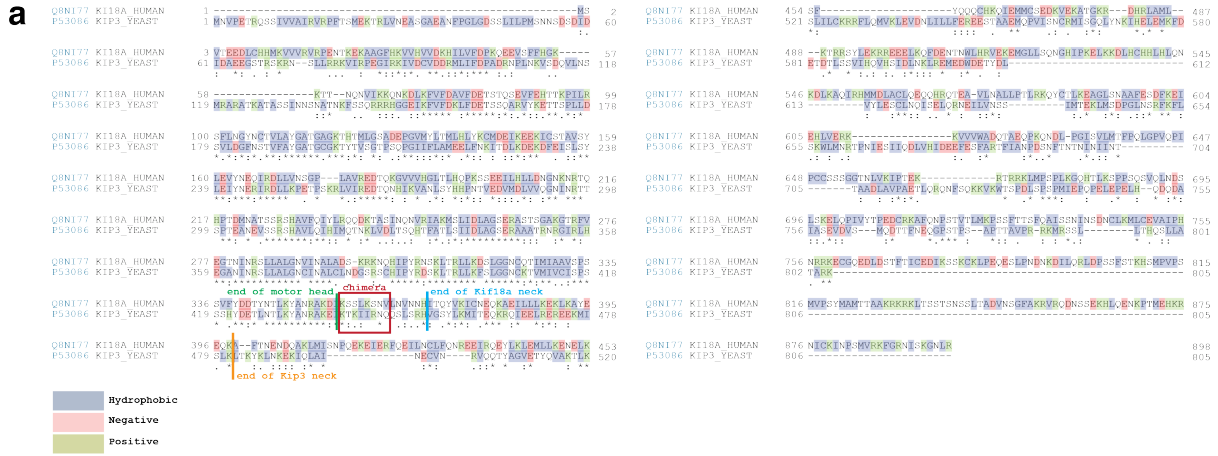

Figure 2.6 Kip3 neck chimera design (a) The mammalian kinesin-8 sequence was aligned to the yeast kinesin-8, Kip3 using Uniprot.org "align" function. The UniProtIDs are shown on the left, Q8N177 for Kif18a and P53086 for Kip3. Each colored box around an amino acid denotes if it is hydrophobic, negative, or positively charged. A star under the alignment denotes a perfect amino acid match, one circle means they are somewhat similar, and two circles are very similar. Additionally, there is an annotation showing the end of the motor heads, the end of the Kif18a neck, and the end of the Kip3 neck. The red box shows the region of Kip3 that was mutated to match the Kif18a sequence.

2.2.4 Kip3 and Stu2 work together for proper metaphase spindle and kinetochore organization

Although the reconstitution experiments described above make possible determining the behavior of different proteins on single yeast microtubules in a cell-cycle specific manner, in the mitotic spindle, microtubule geometry and spindle forces are expected to influence protein behaviors (Trupinić *et al.*, 2022). Therefore, we tested how Kip3 and Stu2 affect kinetochore biorientation in intact spindles within live cells and compared these phenotypes to those detected in our reconstitution assay. As we reported previously, loss of Kip3 results in an increased frequency of kinetochores being declustered along the spindle axis (Torvi *et al.*, 2022) (Figure 2.7a and b). We hypothesized that this declustered phenotype is the result of an increased frequency of laterally bound kinetochores that fail to congress to the microtubule plus-end (Figure 2.1). We now report observing declustered kinetochores in cells expressing Kip3^{NC}, indicating that this phenotype is the result of immobile kinetochores and not the result of defective Kip3 motility (Figure 2.7a and b).

While Stu2 depletion in our assay resulted in immobile kinetochores, Stu2's role as a microtubule polymerase also leads to very short, slowly growing microtubules. This microtubule phenotype is also seen in mitotic spindles of *stu2* mutants (Miller, Asbury and Biggins, 2016) (Figure 2.7b). However, in the absence of Stu2, the frequency of

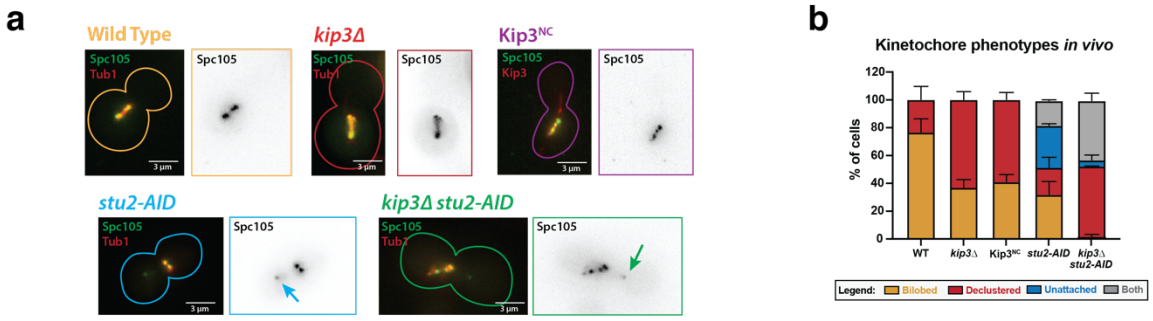

Figure 2.7 Kip3 and Stu2 work together to achieve proper metaphase spindle and kinetochore organization (a) Metaphase cells with either wild-type *KIP3* and *STU2* alleles, or *kip3*Δ, *kip3*^{NC}*, stu2-AID,* and *kip3 & stu2-AID* alleles, were imaged in a *cdc23-1* strain expressing Spc105-GFP (green) and either mRuby2-Tub1 (red). Note that these cells were not shifted to non-permissive temperature and were not arrested in the cell cycle for imaging because the bud morphology indicates the cell cycle stage. Each image shown is a maximum Z-projection of a 5 µm stack of 0.2 µm slices. (b) Quantification of the declustered and unattached kinetochore phenotype is presented as a bar graph for spindles that are 2–3 µm in length. Cells were classified as 'bilobed' by a line scan showing two distinct peaks (represented in the wild-type image). The 'declustered' phenotype included all line scans that did not show two distinct peaks (represented in the *kip3Δ* image). The 'unattached' phenotype was classified as the presence of at least one kinetochore signal off axis away from the main spindle (represented in the *stu2-AID* image). The 'both' classification represents spindles that were both declustered and that had an unattached kinetochore (represented in the *kip3Δ & stu2-AID* image). Two biological replicates were analyzed, each with n=50 cells. Error bars are standard errors of the mean.

unattached kinetochores increased, as reflected in appearance of kinetochore spots far off-axis with the spindle. Additionally, these cells often show both a declustered kinetochore phenotype (more than two kinetochore puncta on axis with the microtubules) and the unattached kinetochore phenotype (Figure 2.7a and b). Together, these phenotypes both affirm Stu2's role in kinetochore attachment (Miller, Asbury and Biggins, 2016) and suggest a novel role in chromosome congression (this study).

Given that loss of Kip3 or Stu2 results in both immobile kinetochores and kinetochore biorientation defects, we sought to gain further insights into how these two proteins work together to facilitate formation of proper kinetochore-microtubule attachments. While the dynamics of these two proteins on microtubules are distinct, and their loss results in different spindle phenotypes, they share a common role in kinetochore congression and biorientation. Therefore, we hypothesized that the simultaneous loss of the two proteins might result in a more dramatic biorientation and spindle defect than either single mutant alone. Strikingly, *kip3Δ stu2-AID* cells completely unable to form bilobed kinetochore puncta. All cells had declustered kinetochores with about half also having at least one unattached kinetochore (Figure 2.7a and b). This result supports the conclusion (Figure 2.8) that these two proteins share a role in facilitating kinetochore congression and biorientation.

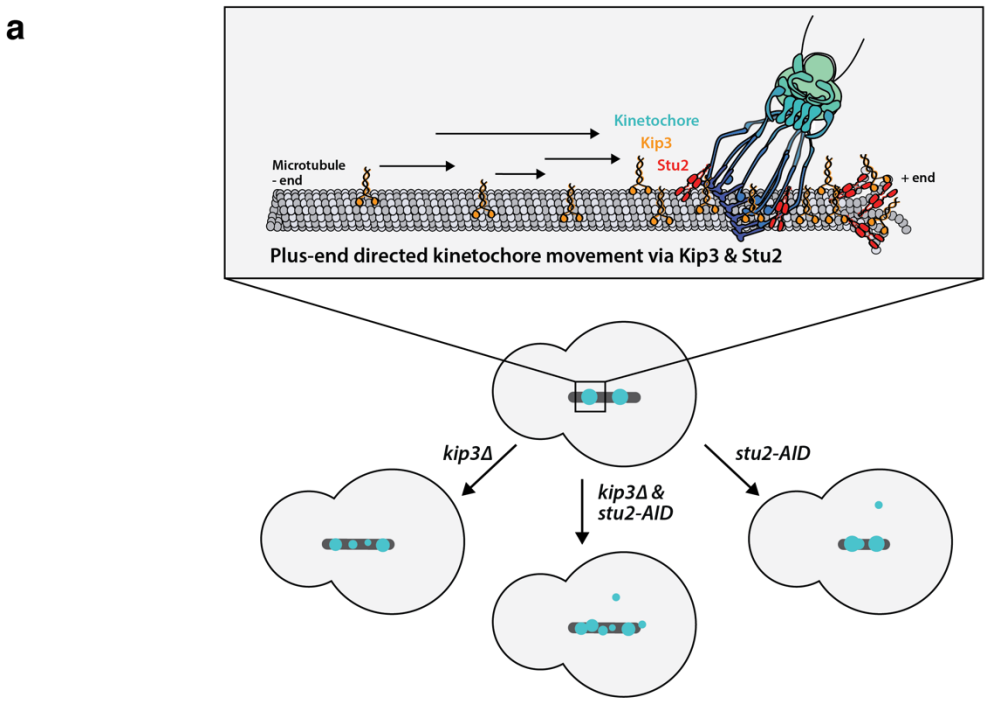

Figure 2.8 Model for Kip3 and Stu2 mediated kinetochore motility (a) Laterally-bound kinetochores travel in a directional manner to the plus end of the microtubule, powered by the kinesin-8, Kip3, and the microtubule polymerase, Stu2. In cells, the loss of these alleles results in kinetochore clustering and chromosome congression defects. Together the *in vitro* and *in vivo* data suggests the importance of Stu2 and Kip3 is forming proper end-on kinetochore-microtubule attachments.

2.3 Conclusion

For chromosomes to be properly segregated to two daughter cells during mitosis, they must first be aligned at the spindle equator, with each sister chromatid attached to an opposing pole via kinetochore microtubules. Establishment of this configuration through chromosome congression and biorientation, must occur efficiently and accurately to ensure genetic continuity through generations and cellular fitness. Although mitosis has been studied in budding yeast and many other cell types extensively, there are many details of congression that have yet to be elucidated. Due to the compact and crowded nature of the mitotic spindle, it is difficult to visualize individual kinetochore-microtubule attachments using light microscopy, which would be required to describe chromosome congression in detail. The use of a lysate-based reconstitution system from cell-cycle synchronized yeast gave us the unique ability to observe dynamics of mitotic proteins on single microtubules while retaining the complexity of the soluble cellular environment. Consequently, our study was able to shed more light on the mechanism of kinetochore-microtubule attachment and biorientation.

Both Kip3 and Stu2 are required for lateral kinetochore movement on microtubules in metaphase lysates; whereupon reaching the tip, they form end-on attachments (Figure 2.1). While Kip3 moves much faster than kinetochores in our assay

(Figure 2.2), Stu2 always localizes with the laterally-bound kinetochores, even when Kip3 is absent from the lysate (Figure 2.4a and b). Because Stu2 had previously been shown to bind to Kip3, it is a candidate to connect Kip3 to the kinetochore. Adding more credence to the possibility that Kip3 associates with kinetochores is the observation that when six amino acids in the neck of Kip3 ($Kip3^{NC}$), that have been shown to be part of the Stu2-binding region (Gandhi *et al.*, 2011), are mutated to the residues of a mammalian kinesin-8, Kif18a, kinetochores no longer move along the microtubule, even though Kip3 velocity remains unchanged (Figure 2.4c and d). Of note, $Kip3^{NC}$ does not accumulate on the tips of microtubules and plus-end dynamics shift toward growth and away from depolymerization in *kip3^{NC}* mutants. These observations are consistent with the possibility that these six amino acids might also be important for Kip3's ability to bind to curved tubulin subunits present at depolymerizing microtubule ends (Arellano-Santoyo *et al.*, 2021; Queen *et al.*, 2023). Another possibility is that Kip3 needs to physically interact with Stu2 at plus ends to accumulate there since loss of Kip3 accumulation at microtubule ends was also observed in *stu2-AID* lysates. In the future it will be important to test these models.

Our evidence indicates that Stu2's function in kinetochore motility is more complex than simply serving as a link between Kip3 and the kinetochore. While Stu2 depletion from lysates resulted in immobile kinetochores (Figure 2.1), Kip3 dynamics were also dramatically altered (Figure 2.4c and d). While a direct effect of Stu2 on Kip3 motor activity has not been demonstrated, evidence for a direct physical interaction between the two proteins in this and previous studies warrant tests of this possibility (Figure 2.4a and b) (Gandhi *et al.*, 2011). Complicating matters further is that the localization patterns for Stu2 and Kip3 on the microtubule are clearly different (Figure 2.2). One possibility is that Kip3 is stably recruited to kinetochores by Stu2, but the signal is too faint for detection. Another possibility is that Kip3 association with kinetochores is too transient for detection. However, we can conclude that Kip3 motility is directly related to the presence of Stu2 in the extract. When we started with lysates from either strains expressing wild-type Stu2 or depleted for Stu2 using *stu2-AID*, Kip3 motility was instantly altered upon replacement with the other lysate (Figure 2.5). It is possible that Stu2 is necessary for activating Kip3, or that Stu2 binding alters Kip3 structure in a way that promotes processivity. The possibility that Stu2 binding alters Kip3 conformation is interesting since Stu2's proposed binding site is in the Kip3 neck-linker (Gandhi *et al.*, 2011), which has recently been shown to be conformationally important for motility (Arellano-Santoyo *et al.*, 2021; Queen *et al.*, 2023). However, validation of these hypotheses will require further testing. Overall, since the essential function of Stu2 is tied to its nuclear localization but is independent of its microtubule polymerase activity (Carrier *et al.*, 2022), its function at kinetochores is likely to be important for cell proliferation.

Another layer of complexity is the correlation between impaired Kip3 processivity and immobile kinetochores. Both in *stu2-AID* lysates (Figure 2.1 and 2.4) and in wild-type lysates arrested in S-phase and anaphase (Figure 2.3a), conditions under which Kip3 makes short runs, kinetochores do not move along the microtubule surface. These cell cycle-dependent differences in the motor activity profile of Kip3 could explain why

kinetochores are only motile in metaphase lysates (Torvi *et al.*, 2022). We speculate that cell cycle-specific post translational modifications might affect Kip3's binding to Stu2, the microtubule, or both. Cell cycle specific phosphorylation of Kip3 has been reported (Woodruff, Drubin and Barnes, 2010; Mieck, 2012). However, site-specific phosphorylation and the direct effects on Kip3's dynamics have not been studied in this context. It is clear that both Kip3 and Stu2 are significant components in the mechanism of kinetochore motility and are regulated by the cell-cycle. While additional studies are needed to clearly elucidate Kip3's and Stu2's exact molecular mechanism, our data provides novel insights into their roles in chromosome congression.

2.4 Material and Methods

2.4.1 Yeast strains, culturing, and harvesting

Yeast strains used in this study are listed in Table S1. Fluorescent protein fusion tags, degradation tags, and deletion constructs were designed and inserted as described previously (Longtine *et al.*, 1998; Lee, Lim and Thorn, 2013; Bindels *et al.*, 2017). Strains were grown in yeast extract peptone dextrose (YPD) rich medium at 25ºC because they contain a temperature-sensitive allele.

Cells were harvested as described previously (Bergman *et al.*, 2018; Torvi *et al.*, 2022). Starter cultures were grown overnight and then diluted into two 2L cultures of YPD at an OD600=$6.25x10^{-3}$. At an OD600=0.4 cultures were shifted to 37ºC for a 3-hour arrest. To specifically degrade a protein of interest, strains containing a degron tag were arrested at 30ºC for 3 hours (total) and then treated with 250 µM 3-indole acetic acid (Sigma-Alrich, St. Louis, MO) for 30 minutes before harvesting. Cells were harvested by centrifugation at 6000 x g in a Sorvall RC5B centrifuge using an SLA-3000 rotor for 10 minutes at 4ºC. Cell pellets were then resuspended in cold ddH2O and pelted in a Hermle Z446K centrifuge for 3 mins at 3430 x g at 4ºC. This last wash step was repeated once more, with any remaining liquid removed from the pellet via aspiration. The cells were then scraped into a 50 mL conical tube filled with liquid nitrogen, snap-freezing them, for storage at -80ºC.

2.4.2 Generation of whole cell lysates

As described previously (Bergman *et al.*, 2018; Torvi *et al.*, 2022), approximately 5g of frozen cells were weighed into a pre-chilled medium-sized SPEX 6870 freezer mill vial (Spex, Metuchen, NJ). The chamber was then cryo-milled as follows: 3-minute pre-chill, 10 cycles of 3 minutes grinding at 30 impacts per second (15 cps), with 1 minute of rest between grinds. The resulting powered lysate was stored at -80ºC and is usable for 2+ years.

2.4.3 Generating stabilized, biotinylated, far-red labeled tubulin seeds

As previously described (Bergman *et al.*, 2018; Torvi *et al.*, 2022), purified bovine tubulin was cycled to enrich assembly-competent tubulin. The tubulin was then mixed with both biotin-conjugated and HiLyte 647 (far-red) labeled porcine tubulin (Cytoskeleton Inc., Denver, CO) and resuspended in PEM buffer (80 mM PIPES pH 6.9, 1 mM EGTA, 1 mM

MgCl2) to a final concentration of 1.67 mg/mL unlabeled tubulin, 0.33 mg/mL biotin-labeled tubulin, and 0.33 mg/mL far-red labeled tubulin. GMPCPP (Jena Biosciences, Jena, Germany) was added to a final concentration of 1 mM. Aliquots were snap-frozen in liquid nitrogen and stored at -80ºC. Seeds were polymerized immediately prior to use by incubation at 37˚C for 10 minutes.

2.4.4 Preparation of glass sides and passivation of coverslips

To prepare the glass sides for use in flow chambers, we followed the previously described protocol (Bergman *et al.*, 2018; Torvi *et al.*, 2022). Microscope slides (Corning Inc., Corning, NY) were incubated in acetone for 15 minutes, followed by 100% ethanol for 15 minutes. The slides were then air dried and stored in an airtight container.

To prepare coverslips (1.5 thickness, Corning Inc.) for use in flow chambers, they were first cleaned by sonication in acetone for 30 minutes. Coverslips were then soaked for 15 minutes in 100% ethanol. After three thorough rinses in ddH2O, coverslips were submerged for 2 hours in a 2% Hellmanex III solution (Hellma Analytics, Müllheim, Germany). They were then rinsed in ddH2O three times and dried with nitrogen gas. For passivation, a solution was prepared containing a 0.1 mg/mL mixture of PLL(20)-g[3.5]-PEG(2):PEG(3.4)-biotin(50%) (SuSoS AG, Dübendorf, Switzerland), at a ratio of 1:19, in 10 mM HEPES. Coverslips were gently placed on 50 µL drops of this solution on Parafilm and incubated for 1 hour at room temperature in a humid chamber. They were then soaked for 2 minutes in PBS and rinsed in ddH2O for 1 minute. The passivated coverslips were dried with nitrogen gas and stored in an airtight container at 4ºC for a maximum of 3 weeks.

2.4.5 Assembly of flow chamber

The flow chamber for use in the TIRF-based dynamics assay was prepared and assembled following the procedure described in (Bergman *et al.*, 2018; Torvi *et al.*, 2022).

2.4.6 Preparation of cell lysates for dynamics assay

Similar to the procedure described in (Bergman *et al.*, 2018; Torvi *et al.*, 2022), a 1.5 mL Eppendorf tube was pre-chilled in liquid nitrogen and filled with 0.22 g of powdered lysate. A microtubule length of ~ 5 µm is optimal for visualization. To create microtubules of this length, varying volumes of cold 10X PEM (800 mM PIPES pH 6.9, 10 mM MgCl2, 10 mM EGTA) were added to the lysate. Different strains required different buffer volumes to achieve the desired length in the assay (between 2-15 µL). The lysate was then combined with 0.5 µL of Protease Inhibitor Cocktail IV (Calbiochem, San Diego, CA) and 4 µL of 25.5 U/µL benzonase nuclease (EMD Millipore, San Diego, CA, prod. 70746-3, >90% purity) and thawed on ice for 10 minutes. The cleared lysate supernatant was then transferred to pre-chilled polycarbonate ultracentrifuge tubes and cleared of insoluble material by spinning at 34,600 x g for 25 minutes at 4ºC. Finally, 32 µL of the cleared lysate supernatant was flowed into the previously prepared chamber, as described above.

2.4.7 TIRF Microscopy

After adding the clarified lysate supernatant to the prepared chamber, the slides were loaded onto a Nikon Ti2-E inverted microscope with an Oko Labs environmental chamber pre-warmed to 28ºC. Images were collected using a Nikon 60X CFI Apo TIRF objective (NA 1.49) and an Orca Fusion Gen III sCMOS camera (Hamamatsu, Hamamatsu City, Japan) at 1.5X magnification using the Nikon NIS Elements software. A LUNF 4-line laser launch (Nikon Instruments, Melville, NY) and an iLas2 TIRF/FRAP module (Gataca Systems, Massy, France) were used to achieve total internal reflection fluorescence (TIRF), which illuminates the region proximal to the coverslip surface. Images were acquired every 5 seconds for 30 minutes unless otherwise noted.

2.4.8 Sequential lysate flow assays

The procedures for preparing coverslips, slides, flow chambers, and lysates were followed as described above. However, instead of preparing one lysate per genotype, two lysates were prepared side-by-side. To observe initial behavior, 32 µL of the first lysate was flowed through the chamber and imaged for 7.5 minutes. While the slide was still mounted on the microscope, the movie was paused for 1 minute while the second lysate was carefully flowed in to replace the first. Once the lysate was replaced, the movie was restarted, and the same field of view was captured for another 7.5 minutes. Frames were captured every 2.5 seconds for a total of 15 minutes.

2.4.9 *In vivo* live cell microscopy

Cells were grown overnight in YPD medium overnight at 25ºC. The next day, they were diluted into fresh YPD and cultured for approximately four hours (two doublings) at 25ºC until the culture reached log phase (OD600=0.5). The cells were then washed three times with minimal Imaging Medium (synthetic minimal medium supplemented with 20 µg/ml adenine, uracil, L-histadine, and L-methionine; 30 µg/ml L-leucine and L-lysine; and 2% glucose; Sigma-Aldrich) and immobilized on coverslips coated with 0.2 mg/ml concanavalin A. Imaging was performed using a Nikon Ti2-E inverted microscope with an Oko Labs environmental chamber pre-warmed to 25ºC. Images were acquired using a Nikon 60X CFI Apo TIRF objective (NA 1.49) and an Orca Fusion Gen III sCMOS camera (Hamamatsu) at 1.5X magnification using Nikon NIS Elements software. A LUNF 4-line laser launch (Nikon) and an iLas2 TIRF/FRAP module (Gataca Systems) were used for HiLo total internal reflection fluorescence (Tokunaga2008). Images were taken with 0.2 µm slices for a total 5 µm Z-stack.

2.4.10 Image and data analysis

For the microtubule dynamics assay, analysis was as described previously (Bergman *et al.*, 2018; Torvi *et al.*, 2022). Imaging data were analyzed using Fiji software (NIH). Registration to correct for stage drift was applied to the raw data (StackReg; (Thévenaz, Ruttimann and Unser, 1998). Kymographs were generated from all microtubules for which the entire length could be tracked for the entire movie. Kymographs were excluded if the microtubules were crossed or bundled. Data from independent technical

trials and biological replicates from imaging of one strain were pooled, unless indicated otherwise. For quantification of speeds, a minimum threshold of 86.7 nm/min for kinetochore movement rates was established based on the resolution of the kymographs used to measure speed. Kinetochore movements of less than a threshold slope of 2-pixel displacement (144.4 nm) per 10 pixels of time (50 sec) were categorized as "paused". Velocities are reported as the mean with the standard error of the mean. Ratios of fluorescent intensities were quantified from individual kymographs that had been background subtracted and bleach corrected using the Fiji plug-in. Using the Fiji "measure" function, average fluorescence intensities were recorded from a line drawn on either the microtubule tip or lattice. Ratios were determined using Microsoft Excel. Statistical significance was determined using a Kruskal-Wallis test (GraphPad Prism, San Diego, CA). P Values are reported as in the figure captions.

For the live cell imaging analysis, images were analyzed using Fiji (NIH). Maximum intensity Z-projections were made, and bleach corrections were applied, using the "histogram matching" macro. Metaphase cells were identified by the presence of a 2-3 μm spindle at the entrance to the bud neck. Cells were then counted as either "bilobed" or "declustered" based on the presence of two distinct kinetochore puncta. Line scans were performed to assist in this binary classification. If two clear peaks were present, the cell was classified as "bilobed." Any other line scan shape, i.e., 3+ peaks or 1 long kinetochore signal that matched the spindle, was classified as "declustered." Cells with kinetochores that were classified as "unattached" had at least one kinetochore signal away from and off-axis from the spindle, even though the main kinetochore mass was still "bilobed." Cells were classified as "both" if there was at least one unattached kinetochore and the main kinetochore mass was also "declustered." Data are from two independent technical trials of two biological replicates. In each replicate, n = 50 cells were counted. Graphs are of the mean and standard error of the mean (GraphPad Prism).

Chapter Three

Final conclusions and outlook

My mom died of cancer the day that I was supposed to start my very first day of research on mitosis. I have always found that a bit ironic. We write into grants and manuscripts that understanding the fundamental molecular mechanisms of how cells divide is necessary for us to ultimately cure cancer. When I worked at the Fred Hutchinson Cancer Research Center, we always made jokes about how "Cures Start Here." Yet, I am continuously humbled by cell biology. There are so many things we don't understand. And while this might be depressing at times, especially as the loved ones around us succumb to illnesses that we wished we could control, I try to find the beauty within the journey. Over these past years I have been able to explore and follow curiosities with creativity. I have been privileged to uncover small little nuggets of information on such a basic but beautiful cellular process. But that being said, of course there is so much more we don't know. There are so many more questions that this work has led me to ask. For every discovery, three new doors of questions open. So, here are the next three burning questions my thesis work has left me with.

1. Can cell cycle regulation and post-translational modifications tell us more about the mechanism of Kip3-mediated kinetochore motility?
2. How does Stu2 affect Kip3 processivity?
3. And lastly, are we missing a level of regulation *in vitro* by not mimicking the *in vivo* spindle geometry?

Each of these questions is guided by my continuous curiosity about how Kip3, a motor that moves much faster than the kinetochore, is required for kinetochore movement. I believe the answer lies in understanding the molecular mechanism of Kip3 processivity in more detail. This includes how it is regulated by the cell cycle, how it is regulated by binding partners like Stu2, and how microtubule bundling and crosslinking, as is found in the spindle, might affect Kip3 function.

Cell cycle regulation of microtubule-associated proteins

As originally reported (Bergman *et al.*, 2018), when using our reconstitution assay, microtubule dynamics differ depending on the cell cycle at which the cells were arrested before being lysed. Here, we have also shown that kinetochore dynamics and Kip3 dynamics are also different depending on the cell cycle stage. Therefore, we hypothesize that in each of these cell cycle stages there are either differences in protein abundance, or differences in post-translational modifications, which in turn affect protein-protein interactions, or both. To address these different possibilities, we developed a purification protocol to isolate microtubules and microtubule-associated proteins from each cell cycle arrest stage. These samples can then be analyzed by mass-spectrometry, in either a quantitative mass-spectrometry mode, or phospho mass-spectrometry mode. However, the pandemic put this aspect of the project on hold, despite some promising initial results.

By adapting a traditional microtubule pelleting assay, we were able to isolate a relatively clean sample of microtubules with bound proteins from lysates arrested in G1, S-phase, metaphase, and anaphase. We additionally tested asynchronous cultures and a negative control of lysate to which both nocodazole and excess calcium were added to inhibit microtubule polymerization. An outline of our modified pelleting assay is shown below (Figure 3.1). To initiate microtubule growth, we added stabilized porcine microtubule seeds. We also added epothilone, a drug that is very similar to taxol, but in contrast, has been shown to stabilize yeast microtubules. Otherwise, the protocol was a series of gentle washes of the microtubule pellet followed by ultracentrifugation to enrich for microtubules and the associated, bound protein (Figure 3.1).

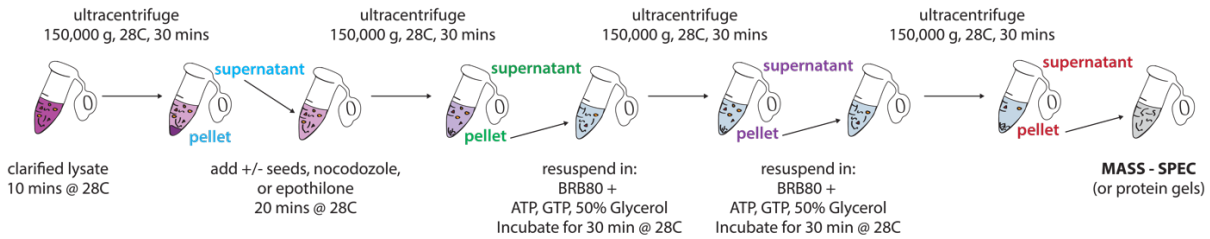

Figure 3.1 Outline of the modified microtubule pelleting assay for mass-spec analysis The clarified lysate from the microtubule dynamics assay was subjected to multiple rounds of ultracentrifugation and washes, as shown here, to enrich for microtubules and associate proteins. Negative control samples received calcium and nocodazole while experimental samples had seeds and epothilone added. Washes were in a gentle BRB80 buffer with ATP, GTP, and glycerol added to also assist in microtubule polymerization. Since yeast microtubules are cold stable, all washes and spins were done at 28C to promote microtubule growth. A sample of each colored label of 'pellet' or 'supernatant' was saved for western and protein gels to monitor protein loss and microtubule enrichment.

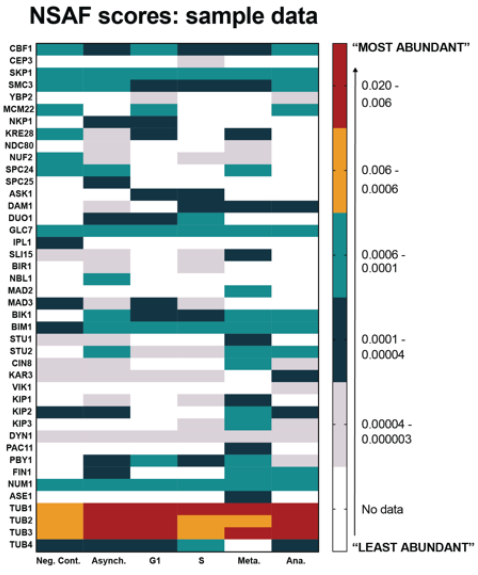

Figure 3.2 Preliminary mass-spectrometry data from the microtubule pelleting assay NSAF scores of sample data are shown as a heat map. Warmer red/yellow colors show proteins in samples that had a higher number and therefore a correlation with a 'higher abundance.' Cooler colors, grays and whites, show samples with either no hits or very low NSAF scores implying a 'lower abundance.' Different samples are shown on the bottom x-axis including the negative control, asynchronous cultures, and lysates arrested in G1, S-phase, metaphase, and anaphase. On the left y-axis are select proteins pulled from the data that were of interest. These include the tubulin proteins, kinetochore proteins, kinesins, and other canonical microtubule associated proteins (Bik1, Bim1, Stu2 etc.).

Only mass spectrometry data from one of our experiments was analyzed before the pandemic hit. However, it showed that we had successfully enriched our sample for microtubules and microtubule-associated proteins. A quick way to determine protein enrichment within mass spectrometry data is through comparing NSAF scores (Michelot *et al.*, 2010). By this approach we were able to show that our samples were enriched for Tub1, Tub2, Tub3, and even some Tub4 (yeast gamma tubulin) (Figure 3.2). The samples were also enriched for kinetochore proteins, motors, and other canonical microtubule-associated proteins (Figure 3.2). Interestingly, we also saw enrichment of some proteins in certain cell cycle stages compared to others. Of particular interest was Kip3 and Stu2 enrichment in samples from metaphase lysates (Figure 3.2). However, these results were preliminary so no conclusion can be drawn other than that this method showed promise. As stated in Conclusions 2.3, there is evidence that Kip3 is phosphorylated by various cell-cycle specific kinases, so the hypothesis that these might affect kinetochore motility is worth pursuing in the future.

Regulation of Kip3 by Stu2

The data in Chapter 2 provide evidence for an important interaction between Kip3, Stu2, and the kinetochore. As stated in Conclusion 2.3, based on our data we believe that Stu2 regulates Kip3's processivity. However, the mechanism is not clear to us. One way in which we could directly test this hypothesis is to turn study purified proteins *in vitro* instead of proteins in the full complexity of lysates. Being able to control the concentrations of both Stu2 and Kip3 in the TIRF chamber, visualize each of these proteins on microtubules, and then quantify dynamics, could reveal the mechanism by which Stu2 activates Kip3. Additionally, we could use these purified proteins to measure binding affinities and other biochemical properties, also giving us insight into the motility mechanism. Lastly, we could make targeted mutations in one or both proteins to identify their binding sites for each other. While the lysate provides and ability to identify novel protein interactions and levels of regulation, now that we know Stu2 affects Kip3's function, a more purified and defined system promises to provide deeper mechanistic insight.

Micropatterning to mimic spindle microtubule geometry

A dream goal has always been to build a mitotic spindle from ground up. Here we have come very close to realizing that dream, reconstituting metaphase-like microtubule arrangements and kinetochore dynamics. However, to me, there has always been one obviously missing part, biorientation. In a spindle, the microtubule geometry is vastly different from what we have on our coverslips. Microtubules are closely packed together, emanating from the spindle pole body. Microtubules are crosslinked both parallel and anti-parallel with respect to one another. Additionally, sister chromosomes are paired and connected via cohesion, which creates tension and a unique set of mitotic spindle forces. Being able to recreate the spindle in our reconstitution system would add another layer of insights into how chromosome congression and Kip3-directed kinetochore motility works in the cell.

As part of my attempts to build the spindle in a TIRF chamber, again before the pandemic hit, I was adapting a protocol involving micropatterning to selectively array

microtubule seeds on glass in pre-designed shapes (Portran, 2014). This protocol involves first developing a photomask with the desired geometries you want the microtubules to acquire. The masks contain small holes of 3-5 μm sizes through which UV light can penetrate. When this mask is placed under UV light with a passivated coverslip underneath, everywhere that light illuminates gets oxidized. The oxidized surface is now the only region to which neutravidin will bind. Therefore, these regions are now the only regions to which biotinylated seeds can bind, resulting in microtubule geometries that have been designed. A schematic of this protocol is outlined below (Figure 3.3a) along with a micrograph containing preliminary data from the reconstitution assay on patterned (Figure 3.3b).

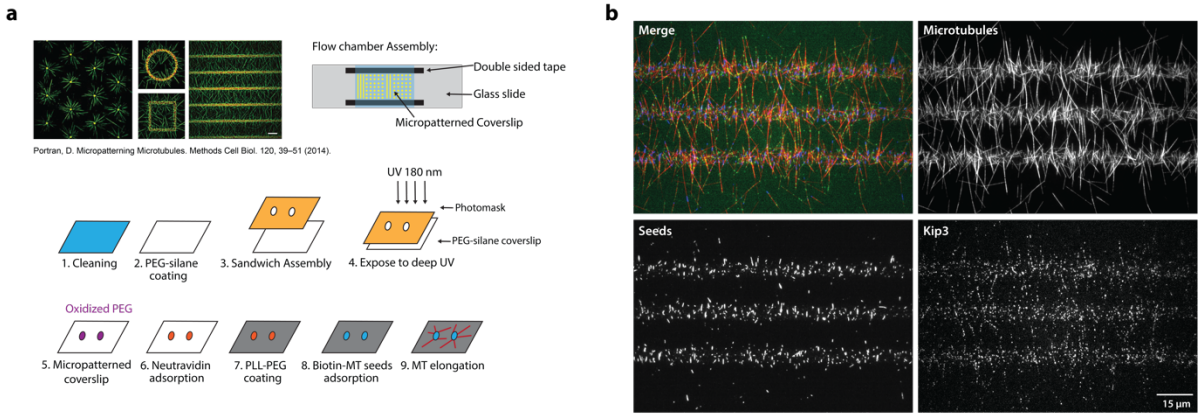

Figure 3.2 Schematic of micropatterning and preliminary data (a) Example data from the publication from which this protocol was adapted is shown on the top left. Next to it is a schematic of what our flow chamber looks. The micropatterned coverslip is placed on a slide and a flow chamber is made with double sided tape. The micropatterned slide is placed in an orientation in which vertical bars span the width of the chamber. This is done to provide the correct orientation while the sample is on the microscope. Below this are the steps for passivating, patterning, and adhering seeds to the coverslip. A coverslip is cleaned and then coated with PEG-silane. Once the coverslip is placed under the photomask and exposed to UV, the PEG becomes oxidized (purple dots). Neutravidin is added and it selectively binds to the oxidized PEG (orange dots now). PLL-PEG is added (gray) to passivate the remainder of the coverslip to prevent non-specific binding. Biotinylated seeds are added and only adhere to the neutravidin (blue now). Next lysate is added and microtubules grow from the seeds patterned on the surface. (b) An example micrograph of the micropatterning working with our lysate. Here are three 3 μm bars where seeds (blue) specifically adhere. Yeast microtubules (red) grow from these seeds, bundling and cross-linking. Kip3 (green) is also along the microtubules.

While I am proud of my thesis and the results presented here, these are just some of the major outstanding questions I am left with at the end of this journey. I wish I understood the mechanism of how Kip3, Stu2, and the kinetochore interact with each other to move the kinetochore in a directional manner. However, with the additional experiments outlined above, I believe we could learn a significant amount more about this mechanism. By doing mass-spectrometry on cell cycle arrested, isolated microtubules and associated proteins, purification of Kip3 and Stu2 with subsequent biochemistry, and micropatterning to recreate natural spindle geometry, perhaps we can answer the question; what is the mechanism of Kip3 chromosome congression and kinetochore motility?

References

Akiyoshi, B. *et al.* (2010) 'Tension directly stabilizes reconstituted kinetochore-microtubule attachments.', *Nature*, 468(7323), pp. 576–9. Available at: https://doi.org/10.1038/nature09594.

Arellano-Santoyo, H. *et al.* (2017) 'A Tubulin Binding Switch Underlies Kip3/Kinesin-8 Depolymerase Activity', *Developmental Cell*, 42(1), pp. 37–51. Available at: https://doi.org/10.1016/j.devcel.2017.06.011.

Arellano-Santoyo, H. *et al.* (2021) 'Multimodal tubulin binding by the yeast kinesin-8, Kip3, underlies its motility and depolymerization', *bioRxiv*, pp. 1–14.

Ayaz, P. *et al.* (2012) 'A TOG:αβ-tubulin Complex Structure Reveals Conformation-Based Mechanisms for a Microtubule Polymerase', *Science*, 337(6096), pp. 857–860. Available at: https://doi.org/10.1126/science.1221698.

Barisic, M. *et al.* (2015) 'Microtubule detyrosination guides chromosomes during mitosis', *Science*, 348(6236), pp. 799–803. Available at: https://doi.org/10.1126/science.aaa5175.

Barisic, M. and Maiato, H. (2016) 'The Tubulin Code: A Navigation System for Chromosomes during Mitosis', *Trends in Cell Biology*, 26(10), pp. 766–775. Available at: https://doi.org/10.1016/j.tcb.2016.06.001.

Bergman, Z.J. *et al.* (2018) 'Microtubule dynamics regulation reconstituted in budding yeast lysates', *Journal of Cell Science*, 132, pp. 1–13. Available at: https://doi.org/10.1242/jcs.219386.

Biggins, S. *et al.* (2013) 'The composition, functions, and regulation of the budding yeast kinetochore', *Genetics*, 194(4), pp. 817–46. Available at: https://doi.org/10.1534/genetics.112.145276.

Bindels, D.S. *et al.* (2017) 'MScarlet: A bright monomeric red fluorescent protein for cellular imaging', *Nature Methods*, 14(1), pp. 53–56. Available at: https://doi.org/10.1038/nmeth.4074.

Carrier, J.S. *et al.* (2022) 'Stimulating microtubule growth is not the essential function of the microtubule polymerase Stu2', *BioRxiv* [Preprint]. Available at: https://doi.org/10.1101/2022.09.09.507218.

Cheeseman, I.M. *et al.* (2006) 'The Conserved KMN Network Constitutes the Core Microtubule-Binding Site of the Kinetochore', *Cell*, 127(5), pp. 983–997. Available at: https://doi.org/10.1016/j.cell.2006.09.039.

Ciferri, C., Musacchio, A. and Petrovic, A. (2007) 'The Ndc80 complex: Hub of kinetochore activity', *FEBS Letters*, 581(15), pp. 2862–2869. Available at: https://doi.org/10.1016/j.febslet.2007.05.012.

Cottingham, F.R. *et al.* (1999) 'Novel roles for Saccharomyces cerevisiae mitotic spindle motors', *Journal of Cell Biology*, 147(2), pp. 335–349. Available at: https://doi.org/10.1083/jcb.147.2.335.

Craske, B. and Welburn, J.P.I. (2020) 'Leaving no-one behind : how CENP-E facilitates chromosome alignment', *Essays in Biochemistry*, 64, pp. 313–324. Available at: https://doi.org/10.1042/EBC20190073.

Edzuka, T. and Goshima, G. (2019) 'Drosophila kinesin-8 stabilizes the kinetochore – microtubule interaction', *Journal of Cell Biology*, 218(2), pp. 474–488.

Fonseca, C.L. *et al.* (2019) 'Mitotic chromosome alignment ensures mitotic fidelity by promoting interchromosomal compaction during anaphase', *Journal of Cell Biology*, 218(4), pp. 1148–1163. Available at: https://doi.org/10.1083/jcb.201807228.

Gandhi, S.R. *et al.* (2011) 'Kinetochore-dependent microtubule rescue ensures their efficient and sustained interactions in early mitosis', *Developmental Cell*, 21(5), pp. 920–933. Available at: https://doi.org/10.1016/j.devcel.2011.09.006.

Gestaut, D.R. *et al.* (2008) 'Phosphoregulation and depolymerization-driven movement of the Dam1 complex do not require ring formation', *Nature Cell Biology*, 10(4), pp. 407–414. Available at: https://doi.org/10.1038/ncb1702.

Geyer, E.A. *et al.* (2018) 'Design principles of a microtubule polymerase', *eLife*, 7. Available at: https://doi.org/10.7554/eLife.34574.

Gonen, S. *et al.* (2012) 'The structure of purified kinetochores reveals multiple microtubule-attachment sites', *Nature Structural & Molecular Biology*, 19(9), pp. 925–929. Available at: https://doi.org/10.1038/nsmb.2358.

Grishchuk, E.L. *et al.* (2008) 'The Dam1 ring binds microtubules strongly enough to be a processive as well as energy-efficient coupler for chromosome motion', *PNAS*, 105(40), pp. 15423–15428.

Gupta, M.L. *et al.* (2006) 'Plus end-specific depolymerase activity of Kip3, a kinesin-8 protein, explains its role in positioning the yeast mitotic spindle', *Nature Cell Biology*, 8(9), pp. 913–923. Available at: https://doi.org/10.1038/ncb1457.

Heald, R. and Khodjakov, A. (2015) ‘Thirty years of search and capture: The complex simplicity of mitotic spindle assembly’, *Journal of Cell Biology*, 211(6), pp. 1103–1111. Available at: https://doi.org/10.1083/jcb.201510015.

Hepperla, A.J. *et al.* (2014) ‘Minus-end-directed kinesin-14 motors align antiparallel microtubules to control metaphase spindle length’, *Developmental Cell*, 31(1), pp. 61–72. Available at: https://doi.org/10.1016/j.devcel.2014.07.023.

Irniger, S. *et al.* (1995) ‘Genes involved in sister chromatid separation are needed for b-type cyclin proteolysis in budding yeast’, *Cell*, 81(2), pp. 269–277. Available at: https://doi.org/10.1016/0092-8674(95)90337-2.

Jenni, S. and Harrison, S.C. (2018) ‘Structure of the DASH/Dam1 complex shows its role at the yeast kinetochore-microtubule interface’, *Science*, 360(6388), pp. 552–558. Available at: https://doi.org/10.1126/science.aar6436.

Kalantzaki, M. *et al.* (2015) ‘Kinetochore-microtubule error correction is driven by differentially regulated interaction modes’, *Nature Cell Biology*, 17(4), pp. 421–433. Available at: https://doi.org/10.1038/ncb3128.

Kapoor, T.M. *et al.* (2006) ‘Chromosomes Can Congress to the Metaphase Plate Before Biorientation’, *Science*, 311, pp. 388–392. Available at: https://doi.org/10.1126/science.1122142.

Kim, H., Fonseca, C. and Stumpff, J. (2014) ‘A unique kinesin-8 surface loop provides specificity for chromosome alignment’, *Molecular Biology of the Cell*, 25(21), pp. 3319–3329. Available at: https://doi.org/10.1091/mbc.E14-06-1132.

Klementieva, N.V. *et al.* (2017) ‘Intrinsic blinking of red fluorescent proteins for super-resolution microscopy’, *Chemical Communications*, 53(5), pp. 949–951. Available at: https://doi.org/10.1039/c6cc09200d.

Koshland, D.E., Mitchison, T.J. and Kirschner, M.W. (1988) ‘Polewards chromosome movement driven by microtubule depolymerization in vitro’, *Nature*, 331(6156), pp. 499–504. Available at: https://doi.org/10.1038/331499a0.

Lee, S., Lim, W.A. and Thorn, K.S. (2013) ‘Improved Blue, Green, and Red Fluorescent Protein Tagging Vectors for S. cerevisiae’, *PLoS ONE*. Edited by A.S. Gladfelter, 8(7), p. e67902. Available at: https://doi.org/10.1371/journal.pone.0067902.

Lemura, K. and Tanaka, K. (2015) ‘Chromokinesin Kid and kinetochore kinesin CENP-E differentially support chromosome congression without end-on attachment to microtubules’, *Nature Communications*, 6. Available at: https://doi.org/10.1038/ncomms7447.

Li, Y. *et al.* (2007) 'Kinetochore dynein generates a poleward pulling force to facilitate congression and full chromosome alignment', *Cell Research*, 17(8), pp. 701–712. Available at: https://doi.org/10.1038/cr.2007.65.

Longtine, M.S. *et al.* (1998) 'Additional modules for versatile and economical PCR-based gene deletion and modification in Saccharomyces cerevisiae', *Yeast*, 14(10), pp. 953–961. Available at: https://doi.org/10.1002/(SICI)1097-0061(199807)14:10<953::AID-YEA293>3.0.CO;2-U.

Magidson, V. *et al.* (2015) 'Adaptive changes in the kinetochore architecture facilitate proper spindle assembly', *Nature Cell Biology*, 17(9), pp. 1134–1144. Available at: https://doi.org/10.1038/ncb3223.

Maiato, H. *et al.* (2017) 'Mechanisms of chromosome congression during mitosis', *Biology*, 6(1), pp. 1–56. Available at: https://doi.org/10.3390/biology6010013.

Malaby, H.L.H. *et al.* (2019) 'KIF18A's neck linker permits navigation of microtubule-bound obstacles within the mitotic spindle', *Life Science Alliance*, 2(1). Available at: https://doi.org/10.26508/lsa.201800169.

Mastronarde, D.N. (2005) 'Automated electron microscope tomography using robust prediction of specimen movements', *Journal of Structural Biology*, 152(1), pp. 36–51. Available at: https://doi.org/10.1016/j.jsb.2005.07.007.

Michelot, A. *et al.* (2010) 'Reconstitution and protein composition analysis of endocytic actin patches', *Current biology: CB*, 20(21), pp. 1890–1899. Available at: https://doi.org/10.1016/j.cub.2010.10.016.

Mieck, C. (2012) *Kinesin motor function at the microtubule plus-end*. University of Vienna. Available at: https://core.ac.uk/download/pdf/18263608.pdf.

Miller, M.P. *et al.* (2019) 'Kinetochore-associated Stu2 promotes chromosome biorientation in vivo', *PLoS Genetics*, 15(10). Available at: https://doi.org/10.1371/journal.pgen.1008423.

Miller, M.P., Asbury, C.L. and Biggins, S. (2016) 'A TOG protein confers tension sensitivity to kinetochore-microtubule attachments', *Cell*, 165(6), pp. 1428–1439. Available at: https://doi.org/10.1016/j.cell.2016.04.030.

Miranda, J.J.L. *et al.* (2005) 'The yeast DASH complex forms closed rings on microtubules', *Nature Structural and Molecular Biology*, 12(2), pp. 138–143. Available at: https://doi.org/10.1038/nsmb896.

Ng, C.T. *et al.* (2019) 'Electron cryotomography analysis of Dam1C/DASH at the kinetochore-spindle interface in situ', *Journal of Cell Biology*, 218(2), pp. 455–473. Available at: https://doi.org/10.1083/jcb.201809088.

Portran, D. (2014) ‘Micropatterning microtubules’, *Methods in Cell Biology*, 120, pp. 39–51. Available at: https://doi.org/10.1016/B978-0-12-417136-7.00003-3.

Queen, K.A. *et al.* (2023) ‘Modification of the Neck Linker of KIF18A Alters Microtubule Subpopulation Preference.’, *bioRxiv* [Preprint]. Available at: https://doi.org/10.1101/2023.05.02.539080.

Rieder, C.L. and Alexander, S.P. (1990) ‘Kinetochores are transported poleward along a single astral microtubule during chromosome attachment to the spindle in newt lung cells’, *Journal of Cell Biology*, 110(1), pp. 81–95. Available at: https://doi.org/10.1083/jcb.110.1.81.

Risteski, P. *et al.* (2021) ‘Biomechanics of chromosome alignment at the spindle midplane’, *Current Biology*, 31(10), pp. R574–R585. Available at: https://doi.org/10.1016/j.cub.2021.03.082.

Schur, F.K. (2019) ‘Toward high-resolution in situ structural biology with cryo-electron tomography and subtomogram averaging’, *Current Opinion in Structural Biology*, 58, pp. 1–9. Available at: https://doi.org/10.1016/j.sbi.2019.03.018.

Shimogawa, M.M. *et al.* (2010) ‘Laterally attached kinetochores recruit the checkpoint protein Bub1, but satisfy the spindle checkpoint’, *Cell Cycle*, 9(17), pp. 3619–3628. Available at: https://doi.org/10.4161/cc.9.17.12907.

Stumpff, J. *et al.* (2008) ‘The Kinesin-8 Motor Kif18A Suppresses Kinetochore Movements to Control Mitotic Chromosome Alignment’, *Developmental Cell*, 14(2), pp. 252–262. Available at: https://doi.org/10.1016/J.DEVCEL.2007.11.014.

Stumpff, J. *et al.* (2011) ‘A Tethering Mechanism Controls the Processivity and Kinetochore-Microtubule Plus-End Enrichment of the Kinesin-8 Kif18A’, *Molecular Cell*, 43(5), pp. 764–775. Available at: https://doi.org/10.1016/j.molcel.2011.07.022.

Stumpff, J. *et al.* (2012) ‘Kif18A and Chromokinesins Confine Centromere Movements via Microtubule Growth Suppression and Spatial Control of Kinetochore Tension’, *Developmental Cell*, 22(5), pp. 1017–1029. Available at: https://doi.org/10.1016/j.devcel.2012.02.013.

Su, X. *et al.* (2011) ‘Mechanisms Underlying the Dual-Mode Regulation of Microtubule Dynamics by Kip3/Kinesin-8’, *Molecular Cell*, 43(5), pp. 751–763. Available at: https://doi.org/10.1016/j.molcel.2011.06.027.

Su, X. *et al.* (2013) ‘Microtubule-sliding activity of a kinesin-8 promotes spindle assembly and spindle-length control’, *Nature Cell Biology*, 15(8), pp. 948–957. Available at: https://doi.org/10.1038/ncb2801.

Tanaka, K. *et al.* (2005) 'Molecular mechanisms of kinetochore capture by spindle microtubules', *Nature*, 434, pp. 987–994. Available at: https://doi.org/10.1038/nature03483.

Tanaka, K. (2012) 'Dynamic regulation of kinetochore-microtubule interaction during mitosis', *Journal of Biochemistry*, 152(5), pp. 415–424. Available at: https://doi.org/10.1093/jb/mvs109.

Tanaka, K. (2013) 'Regulatory mechanisms of kinetochore-microtubule interaction in mitosis', *Cellular and Molecular Life Sciences*, 70(4), pp. 559–579. Available at: https://doi.org/10.1007/s00018-012-1057-7.

Tanaka, T.U., Stark, M.J.R. and Tanaka, K. (2005) 'Kinetochore capture and bi-orientation on the mitotic spindle', *Nature Reviews Molecular Cell Biology*, 6(12), pp. 929–942. Available at: https://doi.org/10.1038/nrm1764.

Thévenaz, P., Ruttimann, U.E. and Unser, M. (1998) 'A pyramid approach to subpixel registration based on intensity', *IEEE Transactions on Image Processing*, 7(1), pp. 27–41. Available at: https://doi.org/10.1109/83.650848.

Torvi, J.R. *et al.* (2022) 'Reconstitution of kinetochore motility and microtubule dynamics reveals a role for a kinesin-8 in establishing end-on attachments', *eLife*, pp. 1–24. Available at: https://doi.org/10.7554/eLife.

Trupinić, M. *et al.* (2022) 'The chirality of the mitotic spindle provides a mechanical response to forces and depends on microtubule motors and augmin', *Current Biology*, 32(11), pp. 2480-2493.e6. Available at: https://doi.org/10.1016/j.cub.2022.04.035.

Tytell, J.D. and Sorger, P.K. (2006) 'Analysis of kinesin motor function at budding yeast kinetochores', *Journal of Cell Biology*, 172(6), pp. 861–874. Available at: https://doi.org/10.1083/jcb.200509101.

Wargacki, M.M. *et al.* (2010) 'Kip3, the yeast kinesin-8, is required for clustering of kinetochores at metaphase', *Cell Cycle*, 9(13), pp. 2581–2588. Available at: https://doi.org/10.4161/cc.9.13.12076.

Weaver, B.A.A. and Cleveland, D.W. (2005) 'Decoding the links between mitosis, cancer, and chemotherapy: The mitotic checkpoint, adaptation, and cell death', *Cancer Cell*, 8(1), pp. 7–12. Available at: https://doi.org/10.1016/j.ccr.2005.06.011.

Wei, R.R., Al-Bassam, J. and Harrison, S.C. (2007) 'The Ndc80/HEC1 complex is a contact point for kinetochore-microtubule attachment', *Nature Structural and Molecular Biology*, 14(1), pp. 54–59. Available at: https://doi.org/10.1038/nsmb1186.

Westermann, S. *et al.* (2005) ‘Formation of a dynamic kinetochore-microtubule interface through assembly of the Dam1 ring complex’, *Molecular Cell*, 17(2), pp. 277–290. Available at: https://doi.org/10.1016/j.molcel.2004.12.019.

Westermann, S., Drubin, D.G. and Barnes, G. (2007) ‘Structures and Functions of Yeast Kinetochore Complexes’, *Annual Review of Biochemistry*, 76(1), pp. 563–591. Available at: https://doi.org/10.1146/annurev.biochem.76.052705.160607.

Woodruff, J.B., Drubin, D.G. and Barnes, G. (2010) ‘Mitotic spindle disassembly occurs via distinct subprocesses driven by the anaphase-promoting complex, Aurora B kinase, and kinesin-8’, *Journal of Cell Biology*, 191(4), pp. 795–808. Available at: https://doi.org/10.1083/jcb.201006028.

Zahm, J.A. *et al.* (2021) ‘Structural basis of Stu2 recruitment to yeast kinetochores’, pp. 1–17.